Chapter 6

Catalytic Proton Reduction using a Series of Hexacarbonyl Diiron Hydrogenase Analogues

Hydrogen fuels cells offer one possible alternative to fuel sources used today. Considering the shrinking quantities of fossil fuels available, and the need to prevent further climate change, an efficient and clean fuel is desired. Mimicking the activity of the [FeFe] hydrogenase enzyme in terms of hydrogen production may offer a solution to the problems currently associated with harnessing hydrogen as a fuel. In a bid to achieve similar turnover rates with synthetic models the mechanism of the catalytic proton reduction must be investigated. As a contribution to this ongoing quest, a series of models for the hydrogenase enzyme have been investigated electrochemically and their catalytic activity has been studied in the presence of a weak acid, acetic acid.

*The structures of the complexes **1 – 5** are based on the well-known organometallic model with the formula, $[Fe_2(CO)_6(SCH_2CHRCH_2S)]$ with the sila-substituted complexes **6 – 10** revealing a silicon atom in the place of the central carbon of the dithiolate bridge. All ten compounds exhibit properties in acidic solution indicative of an electrocatalytic process. The sila-substituted derivatives differ from the carbon analogues in that the first step involves the protonation of a basic sulphur atom followed by reduction of the complex. A CECE mechanism is proposed for the sila-substituted complexes with the exception of the tetra-iron hydrogenase model **9** where the different coordination modes and the environment of the bridging silicon atom lead to the tentative proposal of an ECEC mechanism.*

6.1 Introduction

6.1.1 Hydrogen as an Energy Source

The face of energy technology is changing and scientists are striving to find viable alternatives to the current energy sources used today, which rely heavily on the consumption of fossil fuels. This desire to provide innovative, safer and cleaner fuels for producing energy has led to increased interest in molecular hydrogen which may now be considered as an important fuel in future energy technology.[1] Hydrogen is a renewable energy source. Notable advantages of hydrogen fuel cells encompass zero carbon emissions, which in turn will lead to cleaner air and a reduction in the amount of greenhouse gases emitted.[2]

A large amount of catalyst is required for hydrogen fuel cells to operate efficiently. At present elemental platinum is used as the catalyst. There are, however certain disadvantages to using Pt in hydrogen fuel cells: Pt is an expensive metal, the supply of Pt in the earth's crust is quite low and it is geographically limited with most of the metal found in South Africa and Russia. If the demand for hydrogen fuel cells that rely on Pt as a catalyst increases, the current supply/demand ratio will not suffice. A greater demand for this catalyst leads to increased mining and processing of the metal. The implications of this on the environment must also be considered especially in terms of water and air pollution.[3]

The quest for more economic and environmentally friendly electrocatalysts for the production of molecular hydrogen has led scientists back to nature and to the naturally occurring metal hydrogenase enzymes which catalyse hydrogen evolution.[4]

6.1.2 Hydrogenase Enzymes

When producing molecular hydrogen, microorganisms use naturally occurring hydrogenase enzymes to catalyse the reversible reaction, $2H^+ + 2e^- \leftrightarrow H_2$. These enzymes are found in bacteria such as *Clostridium pasteurianum* and *Desulfovibrio desulfuricans*. These enzymes catalyse the reductive generation and oxidative uptake of molecular hydrogen at remarkable rates which has provoked substantial interest

into the study of the catalytic behaviour and molecular mechanisms by which hydrogenase enzymes operate. By understanding the structure of the hydrogenase active sites and the importance of each cofactor and its function, it has been possible to synthesise analogues of the active site and investigate their catalytic activity.[4, 5, 6]

H_2 in itself is relatively inert and as a molecule it neither exhibits redox nor acid base properties. The interesting thing however, is that when coordinated to metals forming metal hydride complexes both redox and acid base activity is observed. This can be seen with the naturally occurring hydrogenase enzymes where the active sites incorporate transition metals such as Fe and Ni.[5] The hydrogenases constitute a diverse group of enzymes and over the last 10 – 15 years the structural cofactors essential in their enzymatic activity have been thoroughly investigated.[1, 4, 5, 7] Two of the most prominent of the hydrogenase enzymes are the heterodimeric [NiFe]-hydrogenase and the homodimeric [FeFe]-hydrogenase which catalyse the oxidation of hydrogen, with the latter involved in the reduction of protons back to hydrogen, Figure 6.1.

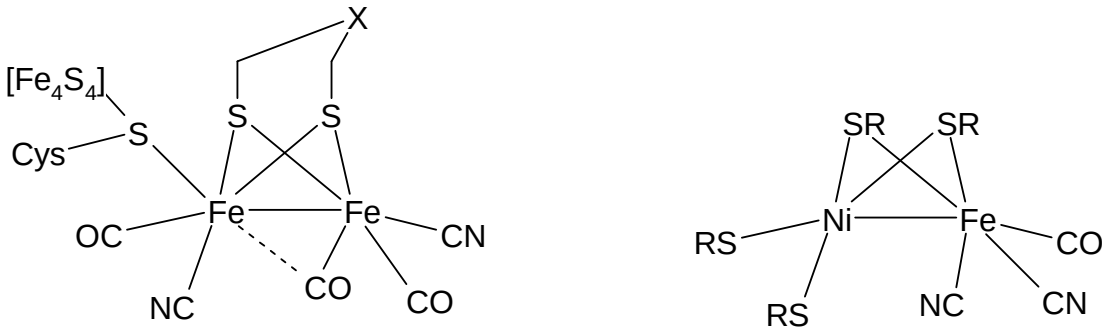

Figure 6.1: *Molecular structure of the [FeFe] and [NiFe] hydrogenases, where R = the amino acid, cysteine.*

Both classes of hydrogenase enzymes contain both carbonyl (CO) and cyanide (CN^-) ligands in their active sites. These diatomic π-acceptor ligands are used to stabilise metals when in low oxidation states. The [NiFe] hydrogenase can be seen to bind to the protein through four cysteinyl ligands (two of which are used to bridge the Ni and

Fe centres) with its Fe-only counterpart binding through one cysteinyl ligand lying close to the [Fe_4S_4] cluster.[7b] In the case of the former, the Fe centre coordinated by the CO and CN^- ligands is diamagnetic and has been detected in the Fe(II) oxidation state, whereas the Ni centre exhibits variable oxidation states. During the catalytic process involved in the oxidation of hydrogen by the [NiFe] hydrogenase a hydride ligand bridges the two metal centres resulting in a change in the geometry of each metal centre.[5] Even though the structure of the [NiFe] hydrogenase is well known, analogues of the active site of the enzyme prove to be synthetically challenging due to the heteronuclear nature of the active site and the unusual structure of the Ni core.[5]

The diiron hydrogenase contains six Fe atoms ('H-cluster') with four of these linked to the active site through a cysteinyl sulphur atom coordinated to the proximal Fe atom, Figure 6.1. Each of the other two octahedrally liganded Fe atoms is coordinated to CO and CN^- ligands with the two Fe centres bridged or semi-bridged by another CO ligand. This CO ligand may interchange between that of a bridging and terminal ligand depending on the state in the enzymatic catalytic pathway.[7a] This diiron active site is also bridged by a dithiolate cofactor where the central atom is thought to be the nitrogen of an amine moiety [8] although this was originally thought to be a $–CH_2$ group.[9] The presence of an oxygen atom in this central atom position cannot be ruled out either.[10] These three different atoms will each have different implications on the electronic nature of the active site as well as the mechanism for evolution of molecular hydrogen. An amine in the central atom position of the dithiolate bridge was proposed based on its ability to act as a base during the catalytic process. Conformational analysis however, disagrees with this idea: a secondary amine group in this position on the dithiolate bridge would be prohibited from taking part in the catalytic process as its preferred conformation would see it involved in hydrogen bonding to the sulphur of the bridging cysteinyl moiety preventing electron delocalisation between the 2Fe active site and the [4Fe4S] subcluster – a factor that is critical in the catalytic process (Figure 6.1).[10]

There is an open site for coordination on the distal Fe centre which may be occupied by a water molecule prior to the proton reduction metabolic process. Whether the water molecule is present or not depends on whether the FeFe hydrogenase is from the *Clostridium pasteurianum* or *Desulfovibrio desulfuricans* bacteria.[10] The active site

for proton reduction in this hydrogenase appears to be located at the Fe centre distal from the $[Fe_4S_4]$ cubane of the H-cluster.[5]

Hydrogen – proton interconversion requires that the active site of the hydrogenase has both a base and a hydride acceptor. The [FeFe] hydrogenase has proven to be more effective than the [NiFe] enzyme in terms of catalysing the reduction of protons to H_2. Several mechanisms for the reduction of protons by the Fe-only hydrogenase have been proposed.[5, 11] One suggestion proposes that the metabolic reaction pathway is activated by reducing the complex and releasing a ligand. It is suggested that the bridging CO ligand moves to a terminal position opening a coordination site between the two Fe centres.[12] A second mechanism suggests that it is the distal iron centre that provides the coordination site for the proton following reduction. The latter mechanism is shown in Figure 6.2, where the 'x' atom of the dithiolate bridge (Figure 6.1) is the carbon of a $–CH_2$ group.

The electronic properties of the coordinated ligands play an important role in the catalytic mechanism. Depending on the electron donating strength of the ligands, the basicity of the Fe centres of the active site may be altered which in turn will determine whether the first step in the catalytic pathway is that of a reduction or a protonation. This initial process can therefore be switched from protonation to reduction, or *vice versa*, by tuning the electronic properties of the ligands coordinated to the Fe centres in the active site and therefore altering the level of basicity. Introducing a basic site in this manner can lead to the first step of the proton reduction mechanism being that of a protonation of the active site, provided the strength of the acid is sufficient. [11a] Protonation, as the first step in the mechanism, is recognised by a positive shift in the reduction potential of the active site whereas in the case of the first step being that of electron transfer into the active site, no change in reduction potential is observed. As pK_a's and reduction potentials are interdependent, addition of an electron to a metal hydride will change the pK_a of the system: [13] the reduced anion is now open to protonation in the presence of an acid, Figure 6.2.

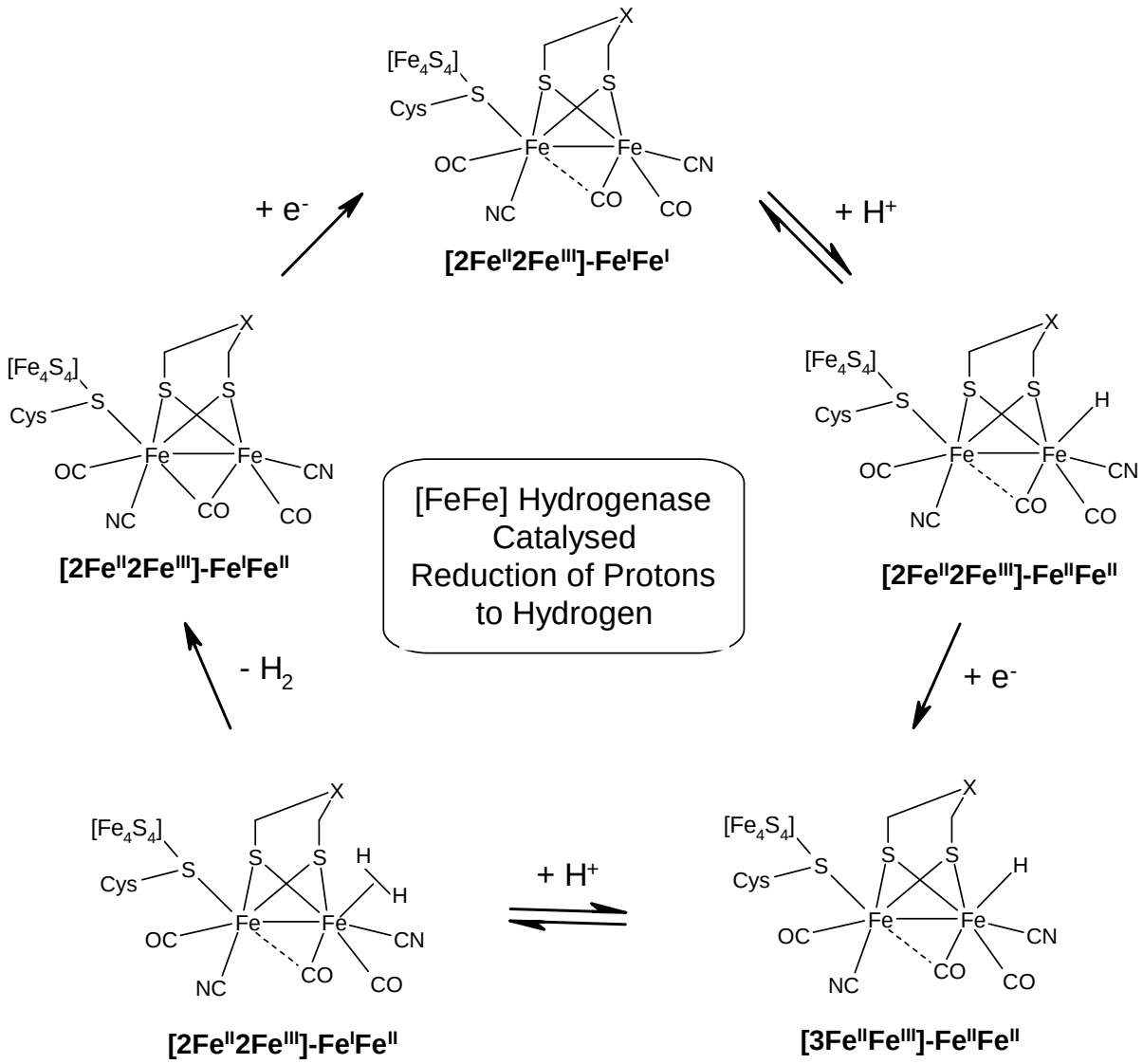

Figure 6.2: *A proposed mechanism for the catalysed reduction of protons using the [FeFe] hydrogenase enzyme.*[11]

6.1.3 Key Cofactors of the [FeFe] Hydrogenases

The cyanide ligands, coordinated to the metal centres within the active site, prove to be one of the most distinguishing characteristics of the hydrogenase enzymes. In the [FeFe] hydrogenase there are two CN^- ligands, one on each of the Fe atoms of the active site whereas in the [NiFe] hydrogenase both of the CN^- ligands are coordinated to the Fe centre only with the Ni metal coordinated to four sulphur atoms, Figure 6.1. The cyanide ligands have a greater tendency to form hydrogen bonds than the carbonyl ligands (which sit in hydrophobic pockets) and this difference between the

two types of hydrogenases may be important in determining the pathway for the metabolic reaction and whether it will involve hydrogen oxidation or production.[8b] To investigate this, diiron dithiolate cyanide salts have been synthesised from derivatives of the [FeFe] hydrogenase of the type, $[Fe_2(SR)_2(CO)_4(CN)_2]^{2-}$. The dicyanide salts formed in this way have a flexible stereochemistry due to a rapid turnstile rotation that is found in complexes of the type $M_2(\mu\text{-}X)_2L_6$. Reactions involving these synthesised dicyanide [FeFe] hydrogenase analogues are not straightforward. However, in the protein this complicated reactivity associated with the cyanide ligand is not observed as a result of hydrogen bonding to amino acids such as serine, lysine and glutamine which protect the active site preventing bimolecular coupling reactions.[5]

The production of molecular hydrogen from protons is facilitated by the redox active 2Fe centre within the H-cluster part of the enzyme. This is assumed to be a two electron process which involves the coupling of two protons accompanied by the reduction of the active site. Within the [FeFe] hydrogenase enzyme the first redox equivalent is given by the 2Fe subcluster with the 4Fe4S cluster providing the second allowing for electrons to be channelled between it and the 2Fe active site. In the enzyme these two subclusters are linked together using a cysteinyl bridge. An analogue of the [FeFe] hydrogenase has been synthesised where the 4Fe4S subcluster is attached to the diiron active site through thiolato bridges allowing for electron communication between the diiron centre and the 4Fe4S cluster.[4] Following reduction of the complex this –SR linkage is ruptured whereas in the hydrogenase enzyme this connection between the two subclusters is protected by the protein.

Intermediates of the metabolic reactions producing H_2 are presumed to consist of hydride derivatives of the enzyme. The hydride may be terminal or bridging (μ-H) and in the case of the enzyme it is thought to be that of the former with the distal iron centre being the coordination site. The presence of the bridging carbonyl in the [FeFe] hydrogenase allows for a vacant site at the diiron subcluster that can house the proton forming a terminal hydride intermediate. Wilson *et al*. have demonstrated that the terminal hydrides exhibit greater reactivity to Brønsted acids than the corresponding μ-H complexes which would suggest that the former are more electron rich and therefore more susceptible to protonation.[14] The terminal hydrides can undergo rapid proceeding reactions forming a μ-H complex. However, this type of follow-up

reaction can be avoided depending on the basicity and asymmetry of the diiron centre.[15] An electron rich diiron centre with bulky ligands allows for a more stable terminal hydride by preventing turnstile rotation and hindering transformation to the μ-H complex. It was initially assumed that the presence of asymmetric Fe centres in the active site of hydrogenase analogues was important for increasing basicity of the centres thereby allowing formation of terminal hydride intermediates in the production of hydrogen. Talamin *et al.* [16] investigated this by synthesising the asymmetric [FeFe] hydrogenase model, $[Fe_2(\mu\text{-pdt})(CO)_4(dppe)]$ (where pdt = propanedithiolate and dppe = diphenyl-P-CH_2-CH_2-P-diphenyl), where NMR experiments were used to detect the presence of terminal hydride intermediates in the protonation of the asymmetric hydrogenase model. Barton and Rauchfuss [15] have reported a symmetrical system mimicking the active site of the [FeFe] hydrogenase, Figure 6.3.

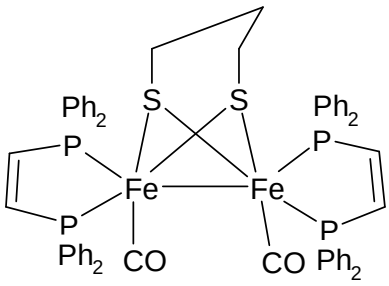

Figure 6.3: *Molecular structure of $[Fe_2(\mu\text{-pdt})(CO)_2(dppe)_2]$, a symmetrical diiron hydrogenase analogue.*[15]

Following protonation, a CO ligand from one of the Fe atoms, moves to a bridging position, between the two iron atoms, resulting in a terminal hydride intermediate. Both the terminal hydride and μ-H derivatives of this hydrogenase analogue catalyse proton reduction releasing H_2 however, the reduction of the terminal hydride is more thermodynamically accessible than that of the bridging hydride. As a result of this the terminal hydride is reduced at potentials approximately 200 mV less negative than the bridging hydride. This proves to be quite an important observation in the development of catalysts for the production of hydrogen in fuel cells as the more thermodynamically accessible the reaction, the less energy required and therefore the more cost effective the catalyst.

6.1.4 Diiron Dithiolato Hexacarbonyl Hydrogenase Analogues

The production of molecular hydrogen using synthetic hydrogenase models is monitored using cyclic voltammetry. The presence of hydrogen evolution from the active site is recognised by the presence of a catalytic current following addition of a proton source – an acid. The criterion for a catalytic current is that the height of the reduction peak increases with increasing acid concentration in the cell. In cases where the first step of the catalytic pathway is a chemical process, i.e. the protonation of the diiron active site, a positive shift in the potential of the cathodic peak is observed following addition of the proton source.

A series of hexacarbonyl diiron hydrogenase analogues have been reported in the literature where the differences, for the most part, lie in the nature of the dithiolate bridge, in terms of the central unit.[6c,d & g, 17] For most of the complexes it is noted that the catalytic hydrogenesis proceeds via electron transfer as the first step of the reaction pathway and an ECEC (electrochemical-chemical-electrochemical-chemical) mechanism is often observed.

In 2003, Darensbourg *et al.* reported the electrocatalytic proton reduction from diiron hexacarbonyl hydrogenase analogues in the presence of a weak acid.[17a]

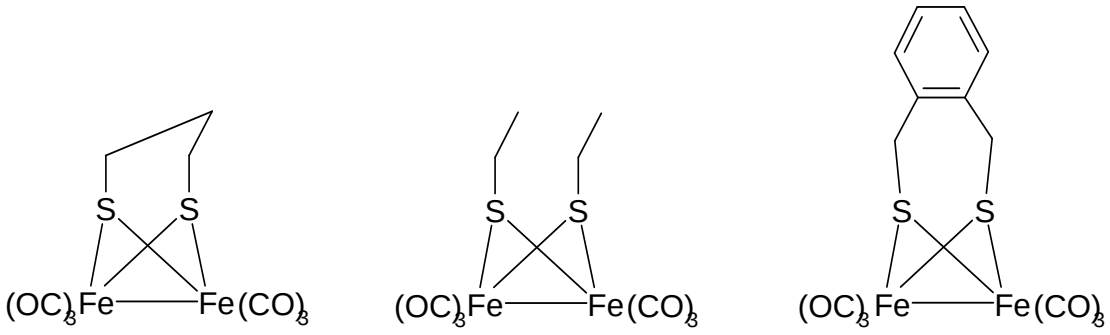

Figure 6.4: *Molecular structures of the hexacarbonyl diiron hydrogenase analogues as reported by Darensbourg et al.* [17a]*, with* $[Fe_2(\mu\text{-pdt})(CO)_6]$ *(left),* $[Fe_2(\mu\text{-}SEt)_2(CO)_6]$ *(middle) and* $[Fe_2(SCH_2\text{-}C_6H_4\text{-}CH_2S)(CO)_6]$.

Two quasi-reversible reduction processes are observed for each of the hexacarbonyl derivatives, Figure 6.4, within the range of -1.16 to -1.34 V (*vs.* NHE). These

reduction potentials are in agreement with similar complexes reported by Pickett *et al.*[18] Initially the complex is in the low valent $Fe^{I}Fe^{I}$ state. Addition of an electron results in the diiron core becoming a mixed valence state with the first reduction corresponding to the one-electron $Fe^{I}Fe^{I} + e^{-} \rightarrow Fe^{I}Fe^{0}$ process. The second reduction process is therefore proposed to correspond to the $Fe^{I}Fe^{0} + e^{-} \rightarrow Fe^{0}Fe^{0}$ process. $[Fe_2(SCH_2\text{-}C_6H_4\text{-}CH_2S\ )(CO)_6]$ is reduced at the least negative potential as the stronger π-acceptor properties of the benzene ring draw electron density away from the diiron core and is therefore the more energetically favourable of the three complexes.[6d] The presence of a linked thiolato bridge is also seen to enhance stability of the reduced species.[19] The production of hydrogen by these complexes was investigated using the weak acid, acetic acid as the proton source. This is in contrast to previous work carried out by Rauchfuss *et al.* [6e, 20] where H_2 production from related complexes was observed using strong acids such as HCl, H_2SO_4 and toluenesulfonic acid with the proposed catalytic mechanism initiated by addition of a proton to the Fe-Fe bond followed by reduction of the complex forming $Fe^{I}(\mu\text{-}H)Fe^{II}$ intermediate and finally releasing H_2. The differing strengths of the different acids used in both cases have an effect on the catalytic pathway with the initial step differing between the strong and weak acids.

Darensbourg *et al.* [17a] observed that the reduction peak potentials do not shift in the positive direction upon addition of acid which would suggest that the initial steps in the catalytic mechanism are electrochemical in nature involving reduction of the complex prior to protonation. A catalytic current is observed originating from the more negative reduction peak representative of an all Fe^{0} complex with formation of the terminal hydride Fe^{II} complex eventually leading to evolution of H_2 from this site. An EECC (electrochemical-electrochemical-chemical-chemical) mechanism is proposed for these hexacarbonyl diiron hydrogenase analogues. This type of catalytic pathway was also observed by Pickett *et al.* [6f] following investigation of $[Fe_2(\mu\text{-}pdt)(CO)_6]$ in the presence of the strong acid, toluenesulfonic acid. Interestingly, the catalytic H_2 evolution process is somewhat inhibited in the presence of excess CO even though the reversibility of the reaction is improved. This behaviour arises as a result of impedance of the catalytically active species due to side reactions forming species where the CO reacts with the diiron catalyst.

The reduction of protons using $[Fe_2(\mu\text{-pdt})(CO)_6]$ as a catalyst involves intermediates of the complex due to side reactions occurring following reduction. The mechanism for hydrogen evolution is less complicated when benzene is used in the dithiolate bridge [6d, 17c] (Figure 6.5) due to the lack of side reactions with the catalyst as confirmed by the chemical reversibility of the complex. The rate of H_2 evolution with this benzene bridged system is however slower than that observed with the pdt bridge complex.[17c]

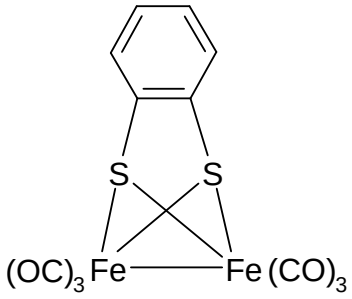

Figure 6.5: *Molecular structure of the diiron hydrogenase analogue, $[Fe_2(\mu S\text{-}C_6H_4\text{-}S)(CO)_6]$.*

The first reduction associated with the benzene-bridged $[Fe_2(\mu S\text{-}C_6H_4\text{-}S)(CO)_6]$ complex corresponds to the addition of two electrons forming $[Fe_2(\mu S\text{-}C_6H_4\text{-}S)(CO)_6]^{2-}$. The systems exhibit a property known as potential inversion, i.e. where the reduction potential of $[Fe_2(\mu S\text{-}C_6H_4\text{-}S)(CO)_6]^{-}$ is less negative that the neutral complex and this results in a two-electron reduction. This $[Fe_2(\mu S\text{-}C_6H_4\text{-}S)(CO)_6]^{2-}$ species is reactive to protons and hence the catalytic cycle begins at this step. An ECEC mechanism is proposed with release of H_2 leading directly back to the catalyst, $[Fe_2(\mu S\text{-}C_6H_4\text{-}S)(CO)_6]$.[6g]

Sun *et al.* [17b] investigated the effect of addition of amino- and nitro- functionalised benzene groups to the azadithiolate bridged (adt) hexacarbonyl diiron complexes, Figure 6.6, on the catalytic proton reduction pathways. The reduction processes observed are akin to those reported for the Darensbourg analogues.[17a] The amino-functionalised derivative is reduced at potentials 140 mV more negative than the

corresponding nitro- complex showing that the two substituents have different effects on the electron density around the diiron core.

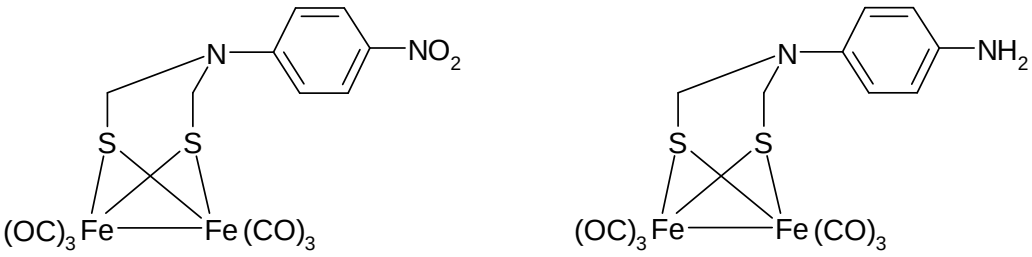

Figure 6.6: *Molecular structures of the amino- and nitro- functionalised hydrogenase analogues, $[Fe_2\{(\mu\text{-}SCH_2)_2N(4\text{-}NO_2C_6H_4)\}(CO)_6]$ (left) and $[Fe_2\{(\mu\text{-}SCH_2)_2N(4\text{-}NH_2C_6H_4)\}(CO)_6]$ (right).*

The catalytic proton reduction of these two complexes was investigated using the weak acid, acetic acid as the proton source. In contrast to the EECC mechanism reported for the carbon bridged hydrogenase analogues [17a] an alternative mechanism for the catalytic production of H_2 is proposed for these adt-bridged complexes. The presence of the nitrogen atom on the dithiolate bridge opens up a basic site in the complex that is susceptible to protonation prior to electrochemical reduction of the diiron active site. This is evident in the shift in the positive direction observed for the first reduction peak following addition of acid. The $[(Fe^0Fe^I)(NH)]$ intermediate is then protonated at the lower-valent Fe atom forming a terminal hydride intermediate, $[(HFe^{II}Fe^I)(NH)]^+$. It is at this point where H_2 evolution is observed and a CECE mechanism is proposed.[17b]

6.1.5 Substituted Diiron Dithiolates

The naturally occurring [FeFe] hydrogenase enzymes have Fe atoms in the active site that are chemically different due to the different ligands coordinated to each of the two iron centres. By replacing one or more CO ligands at the active site in diiron hydrogenase analogues these differentiated environments can be achieved leading to asymmetric complexes that are closely related to the hydrogenase enzyme. Substitution of a CO ligand at the diiron core can affect both the reduction and catalytic properties of hydrogenase analogues. The hydrogenase enzyme contains both

ligands that exhibit π-acceptor properties as well as strong σ-donating ligands. Examples of ligands with σ-donating character are cyanides, substituted phosphorus ligands and N-heterocyclic carbenes. Analogues of the hydrogenase enzyme using these ligands have been reported, Figure 6.7.[6c, 17a, 20, 21]

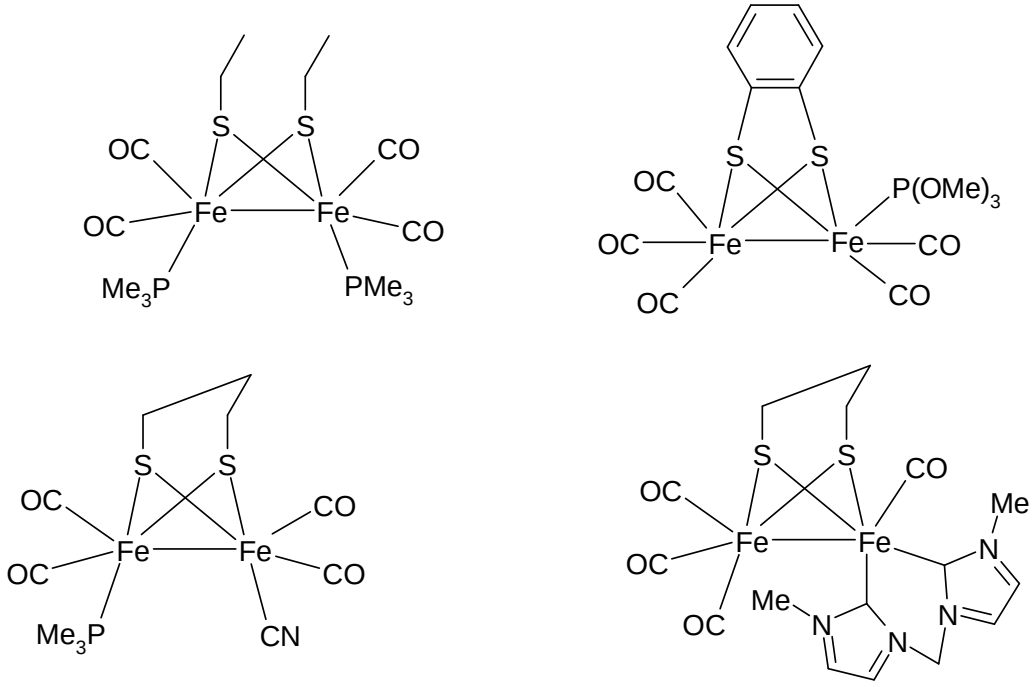

Figure 6.7: *Molecular structures of diiron hydrogenase analogues where one or more CO ligand has been substituted with $[Fe_2(CO)_4(\mu\text{-edt})(PMe_3)_2]$ (top left), $[Fe_2(\mu S\text{-}C_6H_4\text{-}S)(CO)_5(P(OMe)_3)]$ (top right), $[Fe_2(CO)_4(\mu\text{-pdt})(PMe_3)(CN)]$ (bottom left) and $[Fe_2(CO)_4(\mu\text{-pdt})(NHC)_2]$ (bottom right). NHC = 1-methylimidazol-2-ylidene-CH_2-1-methylimidazol-2-ylidene.*

The replacement of a CO ligand by the more electron donating $P(OMe)_3$ ligand, Figure 6.7, leads to more negative reduction potentials of the diiron core as a result of increased electron density around the metal centres as observed in the complex $[Fe_2(\mu S\text{-}C_6H_4\text{-}S)\ (CO)_5\{P(OMe)_3\}]$.[6c] Following the investigation of proton reduction using strong acids a CE mechanism is proposed whereby the complex is first protonated, as noted by the appearance of a new peak at more positive potentials than the reduction of the complex in acid free solution, and this protonated species is then reduced. However, the proton catalysis for this complex is rather slow with only a few turnovers per hour.

Darensbourg *et al*. observed that the PMe_3 substituted complex, $[Fe_2(CO)_4(\mu\text{-edt})(PMe_3)_2]$, exhibits a better response to protons in solution in comparison to the all-CO derivative.[17a] A greater sensitivity to acid concentration was observed as a result of the more stable intermediate of the $[Fe_2(CO)_4(\mu\text{-edt})(PMe_3)_2]$ hydrogenase analogue with 17 turnovers per hour recorded compared to 6 for the all-CO complex. In contrast to the all-CO analogue an ECCE mechanism has been proposed for this complex where initiation occurs at the Fe^IFe^0 oxidation state which is similar to the naturally occurring [FeFe] hydrogenase enzyme. The presence of decent donor ligands stabilise the H-Fe^{II} intermediate allowing for this enhanced catalytic activity from the Fe^0Fe^I state.

In 1999 Rauchfuss *et al.* reported the mixed ligand diiron hydrogenase analogue, $[Fe_2(pdt)(CO)_4(CN)_2]^{2-}$ which exhibited reactivity to protons.[22] This electron rich complex is structurally similar to the diiron hydrogenase enzyme, however, the presence of strong acids in the catalytic reactions greatly affects the stability of the intermediate forming insoluble derivatives of the complex that are catalytically inert. In order to form compounds with less reducing power than $[Fe_2(\mu\text{-pdt})(CO)_4(CN)_2]^{2-}$ and hence greater stability of the protonated intermediate, one of the CN ligands were replaced with a PMe_3 ligand to form $[Fe_2(pdt)(CO)_4(CN)(PMe_3)]^-$, Figure 6.7.[6e] The addition of PMe_3 enhances the basicity of the diiron active site and in the presence of strong acids the complex accepts a proton at one of the Fe atoms of the diiron active site forming the terminal hydride complex, $[HFe_2(pdt)(CO)_4(CN)(PMe_3)]$. The cyanide ligand provides a second protonation site and this complex is an example of how subtle changes in the electronic properties of these types of complexes can significantly alter the catalytic process. Protonation of the Fe-Fe bond as the first step in the catalytic pathway is also observed in the case of the heterocyclic carbene substituted derivative, $[Fe_2(CO)_4(\mu\text{-pdt})(NHC)_2]$ (Figure 6.7).[21] Following addition of acid the first reduction peak is shifted by approximately 100 mV in the positive direction compared to the same peak in the acid free environment. The height of the reduction peak increases linearly with increasing acid concentration which is indicative of a catalytic proton reduction process.

This chapter focuses on a series of diiron hexacarbonyl hydrogenase analogues where the affect of structural changes at the site of the dithiolate bridge on the catalytic

properties of the complexes is investigated. The electrochemical properties and catalytic ability of a series of tetranuclear iron hydrogenase analogues are also examined.

6.2 Results and Discussion

There have been several reports in the literature discussing the nature of the central atom of the dithiolate bridge in the [FeFe] hydrogenase enzyme. Ambiguity still surrounds the identity of this atom and conflicting reports suggest that the two iron atoms in the active site may be bridged by either the alkyl $[(SCH_2)_2CH_2]$ [9] (pdt: 1,3-propanedithiolate), the amino $[(SCH_2)_2NR]$ [8] (adt: azadithiolate) or the ether group $[(SCH_2)_2O]$ [10] (odt: oxadithiolate), Figure 6.8. The effect of changes in the electronic properties of the dithiolate bridge on the catalytic pathways of hydrogen production has been receiving increasing interest over recent years.[15, 23, 24, 25, 26]

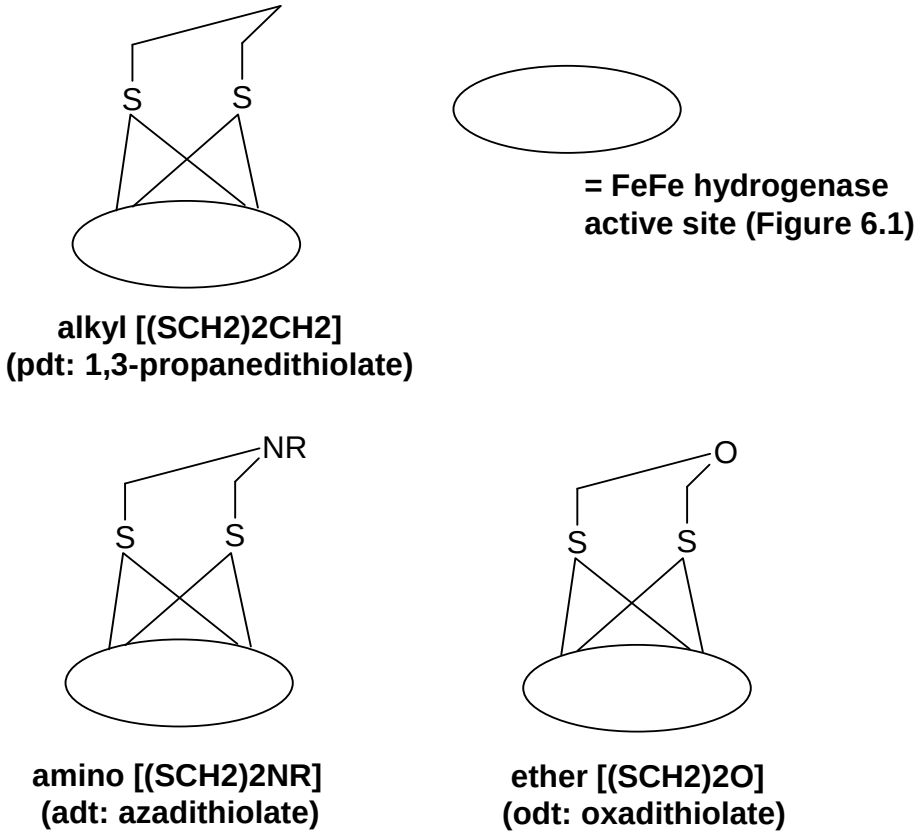

Figure 6.8: *Illustration of the proposed central atoms of the dithiolate bridge within the FeFe hydrogenase enzyme.*[8, 9, 10]

Within the hexacarbonyl diiron complexes each Fe atom obeys the 18-electron rule with closed shell configurations observed in both. This is achieved by the presence of an electron-pair coupling interaction between the two Fe^{I} atoms. These types of

complexes are diamagnetic as a result. The Fe-Fe bond length is relatively short and within the range of a single metal – metal bond. It is proposed that this bond is quite distinct in that it takes on a "bent" conformation.[27] The energy level patterns for the diiron complex, $[Fe_2(CO)_6S_2]$, described by Dahl *et al.* [27] show that the higher filled molecular orbitals (MO) are comprised of three different sets. The upper set (highest in energy of the filled MO's) is made up of 7 filled MO levels that exhibit mostly 3d orbital character. The second and third set of MO levels are of lower energy than this first set with the second set having substantial bridging ligand character with the splitting between the levels of this set being particular sensitive to the nature of the bridging ligand. And finally the third set is proposed to consist of MO's with bridging ligand character or 5σ character arising from the carbonyl ligands.

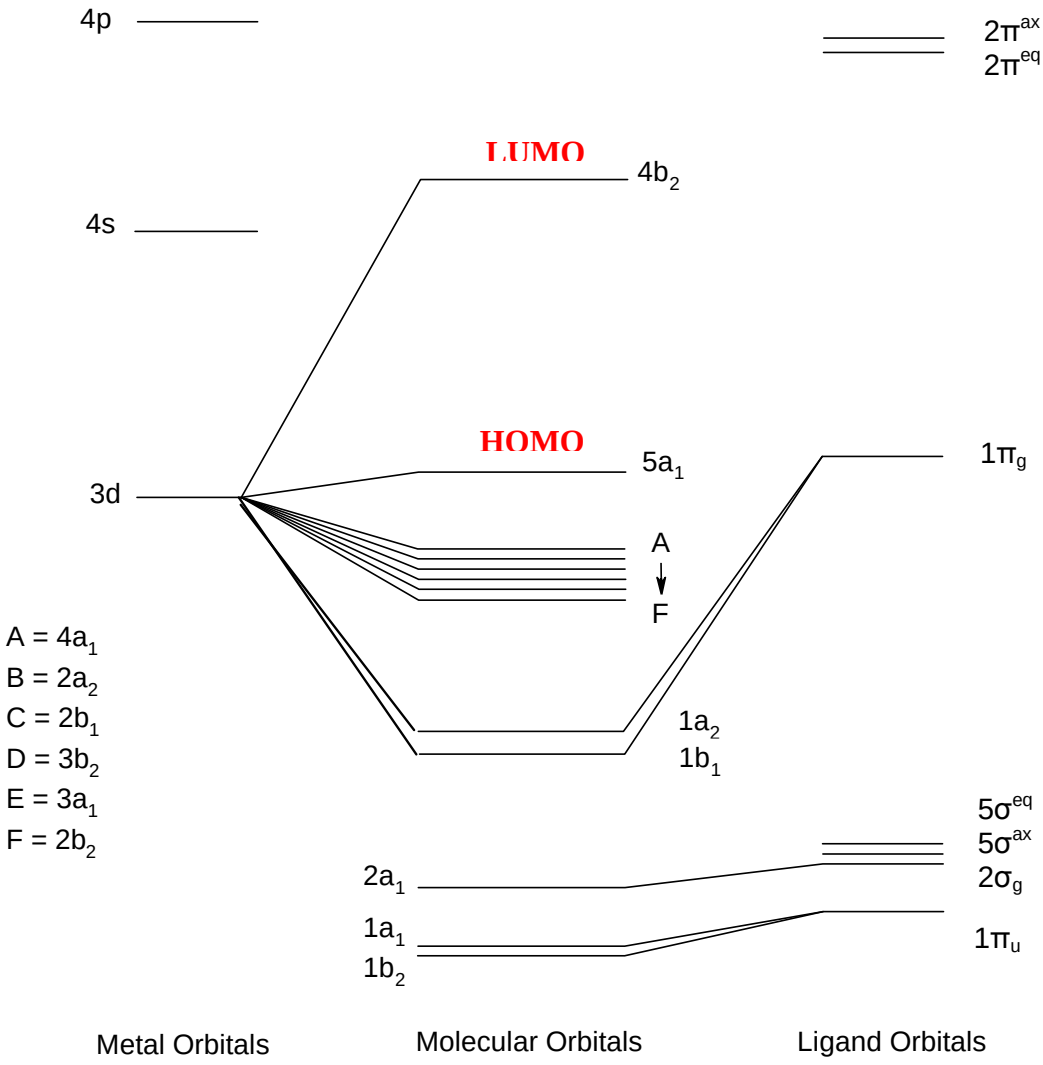

Figure 6.9: *Molecular orbital energy level diagram for a diiron complex with an unsubstituted dithiolate bridge, $[Fe_2(CO)_6S_2]$ as proposed by Dahl et al.*[27]

The HOMO and LUMO levels within the complex correspond to the bonding and antibonding MO's associated with the "bent" Fe-Fe bond. Carbonyl ligands facilitate the stabilisation of the three electron lone pairs on each iron atom (the bonding and antibonding counterparts of which make up the six MO levels below the HOMO) by allowing for back-bonding of charge from the metal into the antibonding 2π CO orbitals. The HOMO is comprised of mostly iron orbital character however; it does contain a small amount of Fe-CO σ-like orbital character which leads to a slight destabilisation of the HOMO with respect to the 3d iron orbitals, Figure 6.9.

To investigate the effect of reduction on the MO's of these types of complexes Dahl *et al.* [27] studied the complex $[Fe_2(CO)_6(PH_2)_2]$ in the neutral, monoanion and dianion states. The low lying LUMO of this complex is quite close in orbital character to the neutral $[Fe_2(CO)_6S_2]$ complex. Upon introduction of a single electron to the LUMO creating the monoanion complex, an increase in the distance of the metal-metal bond is observed which increases further when the complex is further reduced to the dianion. Apart from the sharp decrease in the energy of the LUMO (caused by the increasing length of the Fe-Fe bond) the other energy levels in the complex experience little reordering relative to one another upon introduction of additional electrons into the complex.

The electrochemistry of ten novel complexes is discussed within this chapter. There are structural differences between each complexes in terms of the nature of the dithiolate bridge (with the exception of a selenium analogue, *vide infra*) and therefore any changes in the oxidation or reduction potentials from one complex to the next may be attributed to such changes and their effect on the energy of the associated HOMO and LUMO of the diiron bond.

6.2.1 Hexacarbonyl Diiron Hydrogenase Analogues with a Substituted 1,3-Propanedithiolate (pdt) Bridge

A series of novel [FeFe] hydrogenase analogues $[(Fe(CO)_3)_2(\mu\text{-}SCH_2CHOHCH_2S)]$ (**1**), $[(Fe(CO)_3)_2(\mu\text{-R})]$ where R = 1,3-disulfanyl-2-propyl-tetra-*O*-acetyl-β-D-glucopyranoside (**2**) with the selenium derivative (**3**), $[(Fe(CO)_3)_2(\mu\text{-}SCH_2CHRCH_2S)]$ where R = $-CH_2CH(COO$*t*$\text{-Bu})(NHBoc)$ (**4**) and [{$(Fe(CO)_3)_2(\mu$-

$SCH_2CHRCH_2S)\}_3$] where R = *O*-acetyl-phenyl (**5**) have been examined and their electrochemical properties and catalytic behaviour is discussed herein. The molecular structure of each complex is shown in Figure 6.10.

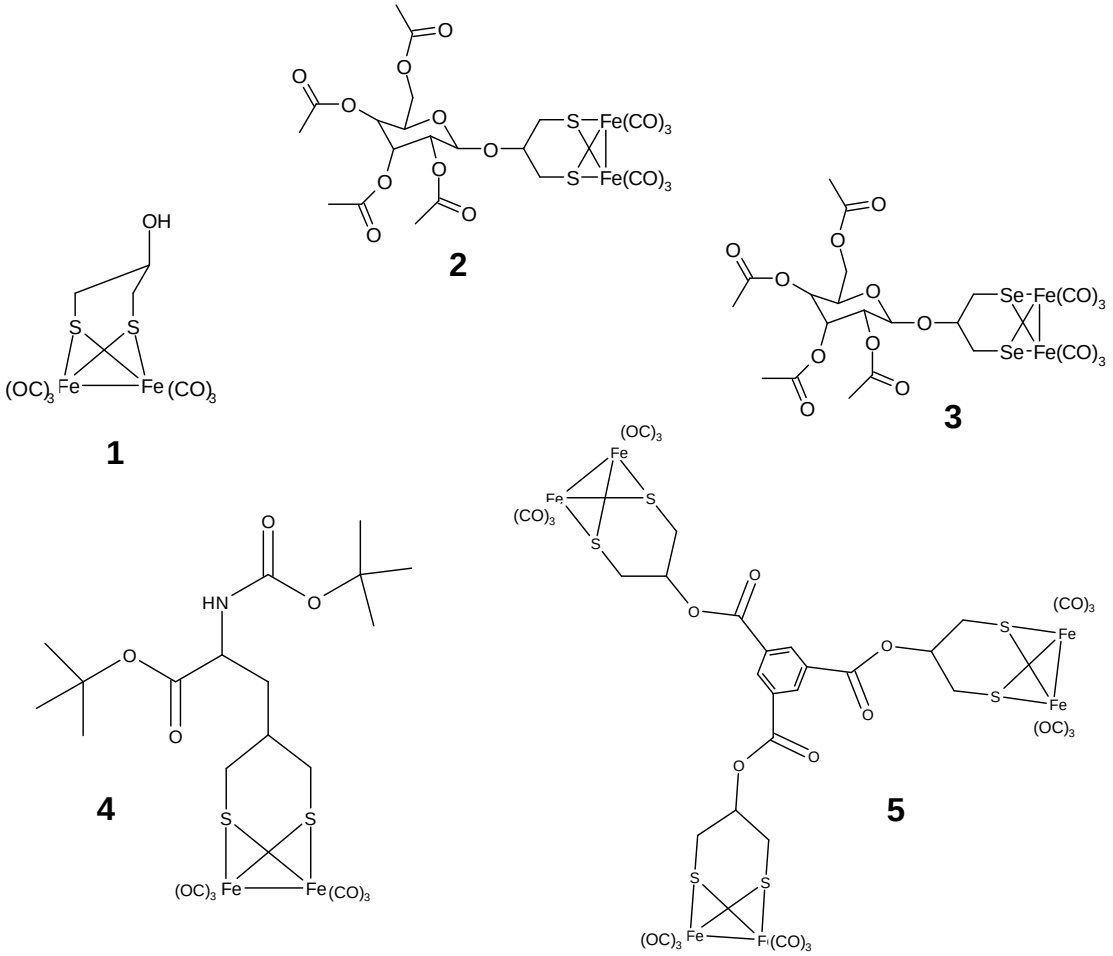

Figure 6.10: *Molecular structures of the diiron hydrogenase analogues **1** – **5**.*

6.2.1.1 Electrochemistry of Substituted pdt-Bridged Hydrogenase Analogues

The electrochemical properties of each complex were examined using cyclic voltammetry and differential pulse voltammetry at a glassy carbon working electrode. The CV of each complex exhibits one anodic wave representing the oxidation of the diiron centre according to the reaction, $Fe^IFe^I \rightarrow Fe^IFe^{II} + e^-$. Two cathodic waves are observed in the CV of each, the potentials of which are detailed in Table 6.1. One anodic and two cathodic waves are also observed for the μ-pdt reference compound,

$[(Fe(CO)_3)_2(SCH_2CH_2CH_2S)]$, Figure 6.4.[17a] The first of these negative peaks corresponds to the $Fe^IFe^I + e^- \rightarrow Fe^IFe^0$ process with a further reductive reaction $Fe^IFe^0 + e^- \rightarrow Fe^0Fe^0$ represented by the second cathodic wave.

Compound	$Fe^IFe^I/Fe^{II}Fe^I$ ***[V]***	Fe^IFe^I/Fe^0Fe^I ***[V]***	Fe^0Fe^I/Fe^0Fe^0 ***[V]***
1	+0.85 (E_{pa})	-1.53 (E_{pc}), -1.42 (E_{pa})	-2.15 (E_{pc})
2	+1.09 (E_{pa})	- 1.50 (E_{pc}) - 1.39 (E_{pa})	- 1.89 (E_{pc})
3	+0.97 (E_{pa})	- 1.46 (E_{pc}) - 1.36 (E_{pa})	- 2.02 (E_{pc})
4	+0.92 (E_{pa})	-1.57 (E_{pc}) -1.47 (E_{pa})	-2.15 (E_{pc})
5	+0.92 (E_{pa})	-1.47 (E_{pc}) -1.37 (E_{pa})	-2.18 (E_{pc})
$[(Fe(CO)_3)_2(\mu\text{-pdt})]$ [17a, b]	+0.84 (E_{pa})	-1.57 (E_{pc}) -1.47 (E_{pa})	-2.11 (E_{pc})

Table 6.1: *Electrochemical data for complexes **1 – 5**, and related compound, at a GC working electrode in acetonitrile, vs. Ag/Ag^+ reference electrode.*

The first (least negative) cathodic peak of all five complexes is indicative of a quasi-reversible reductive process that represents the $Fe^IFe^I + e^- \rightarrow Fe^IFe^0$ process. The peak-peak separation (ΔE_p) is within the range of 100-110 mV which also suggests that the electron transfer is not fully reversible. This quasi-reversible nature has been observed in other complexes containing an all-carbon linker between the two sulphur atoms of the dithiolate bridge.[17a, 28] It is noted that the chemical reversibility of this first reduction is somewhat dependent on the nature of the bridging ligand. By generating a CO saturated solution of the complex an increase in the reversibility of the redox process can be achieved.[6f] A second irreversible wave is observed when a further electron is pumped into the active site of the complex, as indicated by the absence of an anodic wave on the return sweep. The first reduction of the complex occurs by inserting an electron into the antibonding orbital of the Fe-Fe metal bond.[27]

It is thought that this newly created SOMO (singly occupied molecular orbital) can accept a second electron and this further reduction lengthens the metal-metal bond and possibly results in cleavage of the bond followed by a structural reorganization of the complex. The addition of the two electrons to the active site would allow for the 18 electron rule to be obeyed by each Fe atom was the bond to break.[28] Also, the existence of a large difference in potential between the first and second cathodic waves suggests that the location of the sites for each process are not isolated from one another and there is a certain degree of electronic communication within the complex following the addition of the first electron.

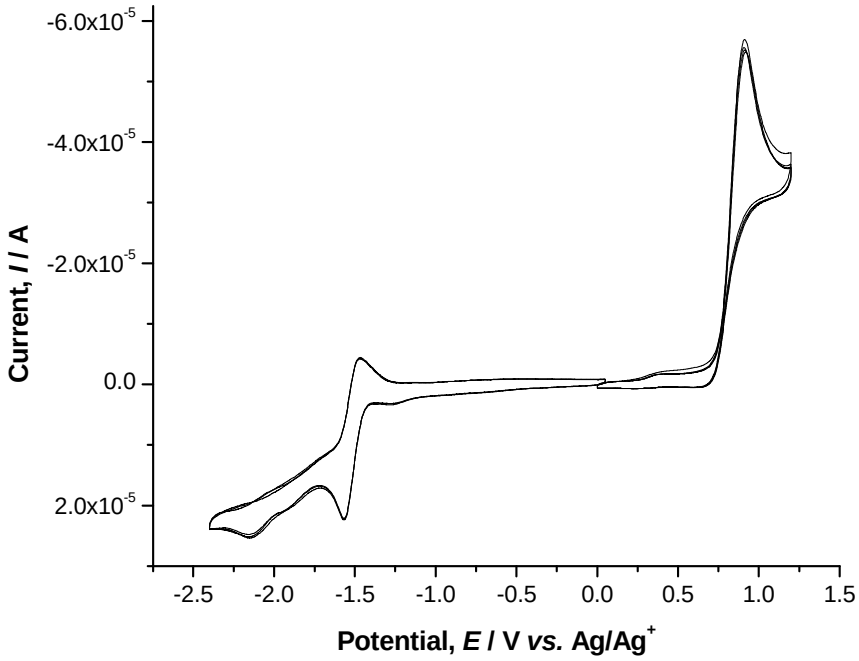

Figure 6.11: *Cyclic voltammetry of complex **4** [1mM], at a GC working electrode (3 mm geometrical diameter), in acetonitrile with 0.05 M $TBAPF_6$ as the supporting electrolyte. Scan rate: 100 mV/s.*

Complex **1** reveals the lowest (least positive) oxidation potential within the five complexes. This potential compares favourably, within experimental error, to that recorded for the diiron μ-pdt complex [17a, b] (Figure 6.4) which suggests that the presence of the hydroxy group in the pdt bridge has a negligible effect on the electron density around the metal centre and consequently the energy of the HOMO located on

the diiron metal bond. The potential of the first reduction process in **1** is 40 mV more positive than the corresponding process in the diiron μ-pdt complex. Therefore the presence of the hydroxyl group may have an effect on the LUMO level within the diiron bond however a shift of 40 mV may be considered to be within the range of experimental error.

By comparing complexes **1** and **2**, it can be seen that the presence of the acetylated sugar on the pdt bridge has a large effect on the diiron centre within the complex. The oxidation potential is shifted by 240 mV in the positive direction suggesting that the large sugar group exhibits strong electron withdrawing character compared to the –OH group in **1**. Making another structural change within the complex closer to the metal centres, by substituting the sulphur atoms of the dithiolate bridge with selenium atoms, leads to a decrease in the oxidation potential by approximately 120 mV suggesting that the stability of the t_{2g} molecular orbitals is greatly effected by the less electronegative selenium atoms. In comparison to the changes observed in the oxidation potentials, minor fluctuations in the reduction potentials of **2** and **3** are observed. What is also interesting is that even though an increase in oxidation potential is observed when comparing complex **2** with that of the more easily oxidised **3**, the same trend is not observed when evaluating the reduction potentials. The different effect of the less electronegative selenium on the oxidation and reduction potentials is not surprising considering Dahl *et al.*'s [27] proposal that the HOMO and LUMO levels are located on the bonding and antibonding orbitals of the bent Fe-Fe bond respectively.

A single irreversible anodic wave has been observed for complex **4** (E_{pa} = +0.92 V, *vs.* Ag/Ag^+) representing the removal of an electron from the HOMO of the complex. A reduction potential similar to those of complex **1** (E_{pc} = -1.53 V) and the diiron μ-pdt complex, Figure 6.4 E_{pc} = -1.57 V, is noted for the first cathodic process where the E_{pc} = -1.57 V, *vs.* Ag/Ag^+. **2**, **3** and **5** are all reduced at potentials less negative than **4** which may result from the presence of the oxygen atom on the substituted dithiolate bridge. Oxygen is more electronegative than carbon and the decrease in electron density around the diiron centre in **2**, **3** and **5** compared to **4** would result in a more positive reduction potential.

The cyclic voltammetry and differential pulse voltammetry of the hexanuclear complex **5**, like **4** also reveals only one anodic process at a potential of +0.92 V (*vs.* Ag/Ag^{+}). The coordination environment of each metal centre within the compound is identical to the next with three CO ligands, two sulphur atoms and a neighbouring Fe atom in its coordination environment. Complexes, with symmetrical metal centres, and a negligible degree of electronic interaction between the centres across a bridging ligand will often only exhibit one anodic wave representing the simultaneous oxidation of the metal centres. This can be seen for complex **5** where the presence of a single peak in the positive region indicates that the three diiron centres are oxidised simultaneously without communication between the three active sites. The exact concentration of this solution in the electrochemical cell was unknown as a result of poor solubility in the organic solvents used in the supporting electrolyte (either dichloromethane or acetonitrile).

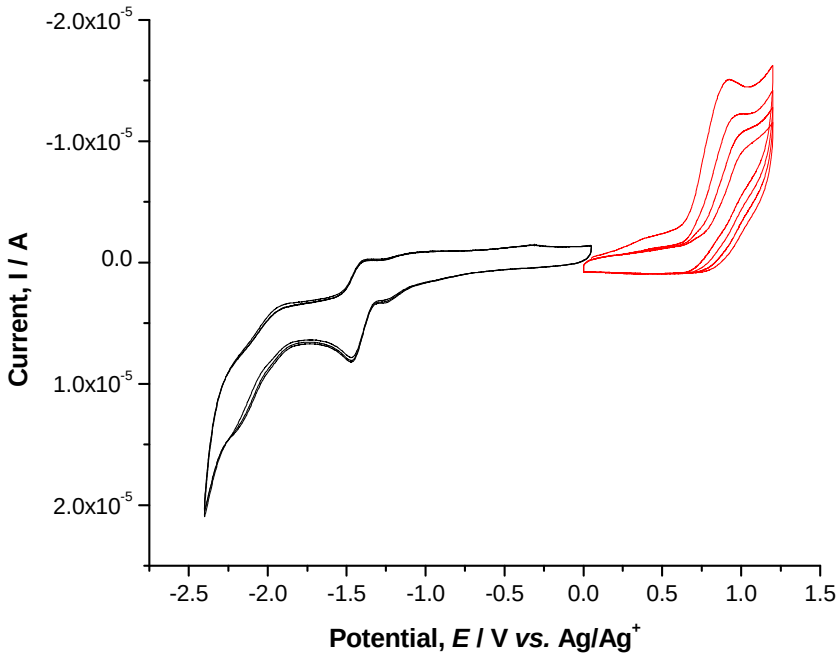

Figure 6.12: *Cyclic voltammetry of complex **5** [<1mM], at a GC working electrode (3 mm geometrical diameter), in acetonitrile/dichloromethane with 0.05 M $TBAPF_6$ as the supporting electrolyte. Scan rate: 100 mV/s.*

When scanning toward positive potentials the oxidised [$Fe^{II}Fe^{I}$] compound appeared to pacify the electrode with each cycle, Figure 6.12. This was evident by the fact that the intensity of the peak current decreased with each consecutive scan and the peak potential was seen to shift to more positive potentials. This process lead to complications in calculating the number of electrons involved in the oxidation of the complex.

6.2.1.2 Electrocatalytic Proton Reduction of Substituted pdt-Bridged Hydrogenase Analogues

The diiron hydrogenase analogues are synthesised with the intention of applying these types of systems to fuel cells to catalyse the reduction of protons to molecular hydrogen. The catalytic potential of each of the five complexes reported above was investigated electrochemically using the weak acid, acetic acid (HOAc), as the proton source. Acetic acid is reduced in acetonitrile at -2.48 V (*vs.* Ag/Ag^{+}). The hydrogenase analogues display the ability to act as these types of catalysts when in the low valent reduced forms, with proton reduction observed either from the [$Fe^{0}Fe^{I}$] or fully reduced [$Fe^{0}Fe^{0}$] states. The catalytic process is examined by adding acid in increments thereby increasing the concentration of acid in the solution with each cycle and monitoring the catalytic reaction electrochemically. When catalysis successfully occurs and protons are reduced to hydrogen the catalytic wave increases in height. A negative shift in the reduction potential of the catalytic wave is also observed on occasion. The reason for this is that the reaction proceeds at such a rate that the current is controlled by diffusion of the substrate in solution into the double layer at the electrode surface.[29] Upon addition of acid an irreversible cathodic process is observed indicating the formation of catalytically active species involved in the mechanistic pathway. The electrocatalytic properties of the diiron complexes discussed in this chapter were investigated by adding a weak acid and monitoring the changes in the electrochemistry.

Monitoring the changes in the reduction potentials in the negative region of the CV of complexes **2 - 5** leads to the observation that there is an absence of a positive shift in the reduction potential of the first redox process ($-1.46 < E_{pc} < -1.57$ V) following the addition of acetic acid. This suggests that the initial step in the mechanistic pathway

involves the reduction of the diiron hydrogenase catalyst to [$Fe^{0}Fe^{I}$] and not the protonation of the complex as has been observed for the azadithiolate (adt) bridged complexes, Figure 6.6, which have a nitrogen atom in the dithiolate bridge as the basic site.[17b]

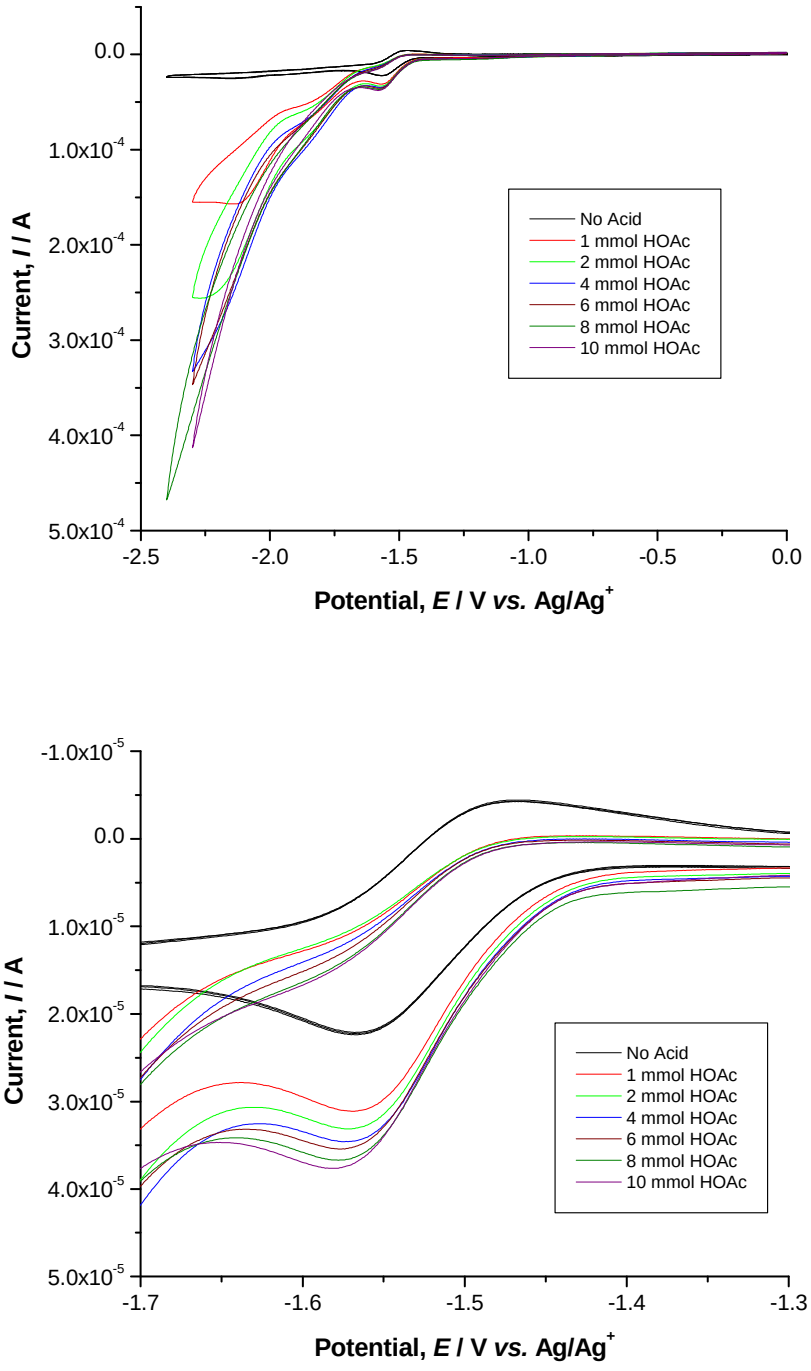

Figure 6.13: *Cyclic voltammetry of* ***4*** *[1 mM] at a GC working electrode, with HOAc (0-10 mmol) using 0.05M $TBAPF_6$ in acetonitrile as the supporting electrolyte. Scan rate: 100 mV/s.*

Upon addition of one equivalent of acetic acid (1 mmol) a small increase in the current intensity of this first reduction wave is observed however, further equivalences of acid added to the system result in minimal changes to the height of this peak, Figure 6.13.

Upon further reduction to the lower valent [Fe^0Fe^0] oxidation state, catalytic behaviour is observed: the height of the peak increases with each increment of acid added and it is also noted that the potential of this cathodic peak does not shift in the positive direction. In fact, the reduction potential of this peak is seen to move ever so slightly further negative with each aliquot of acid. This type of behaviour has been observed for other hexacarbonyl diiron hydrogenase analogues: the formation of molecular hydrogen from the pdt bridged catalyst, [$(Fe(CO)_3)_2(SCH_2CH_2CH_2S)$], is thought to follow an electrochemical-electrochemical-chemical-chemical (EECC) mechanism.[17a]

This type of mechanism is observed when the singly reduced Fe^0Fe^I oxidation state is catalytically inactive and addition of a second electron forming the lower valent Fe^0Fe^0 state is required in order to initiate the catalytic cycle. This [Fe^0Fe^0] state is reactive to protons and an [Fe^0Fe^{II}-H] complex results. Following on from the formation of this hydride complex the oxidised iron centre is now in a position to accept another proton generating the [$(\eta^2\text{-}H_2)Fe^{II}\text{-}Fe^0$] complex according to Scheme 6.1. This type of EECC catalytic pathway is proposed for complexes **2** – **5**.

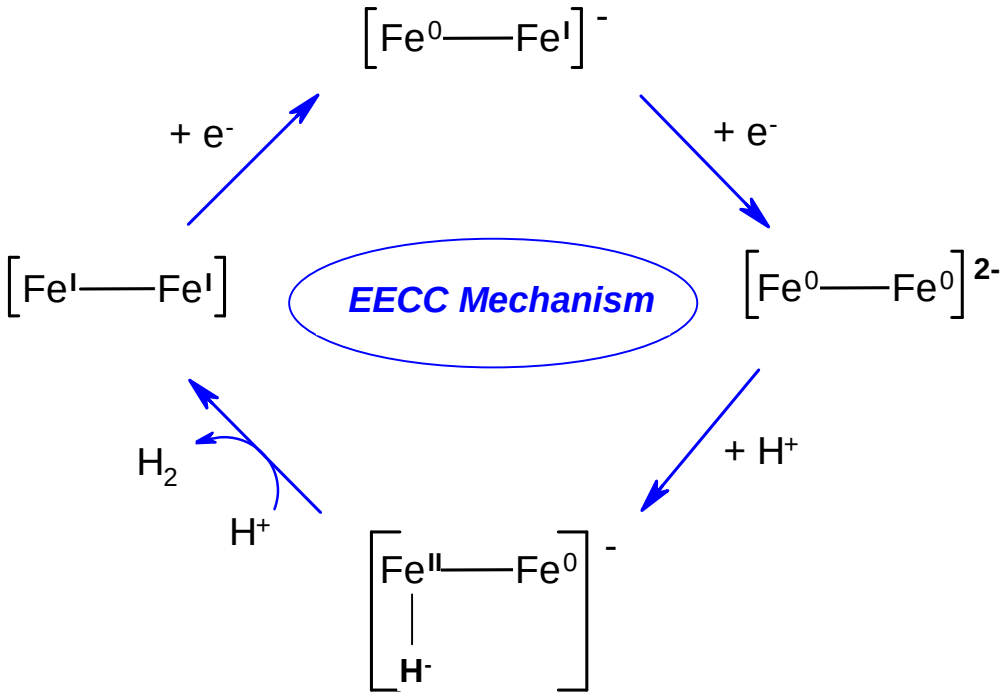

Scheme 6.1: *Proposed EECC mechanism for the electrocatalysis incorporating hexacarbonyl diiron dithiolate complexes* ***2 – 5*** *where the catalytic cycle is initiated from the second reduction step.*

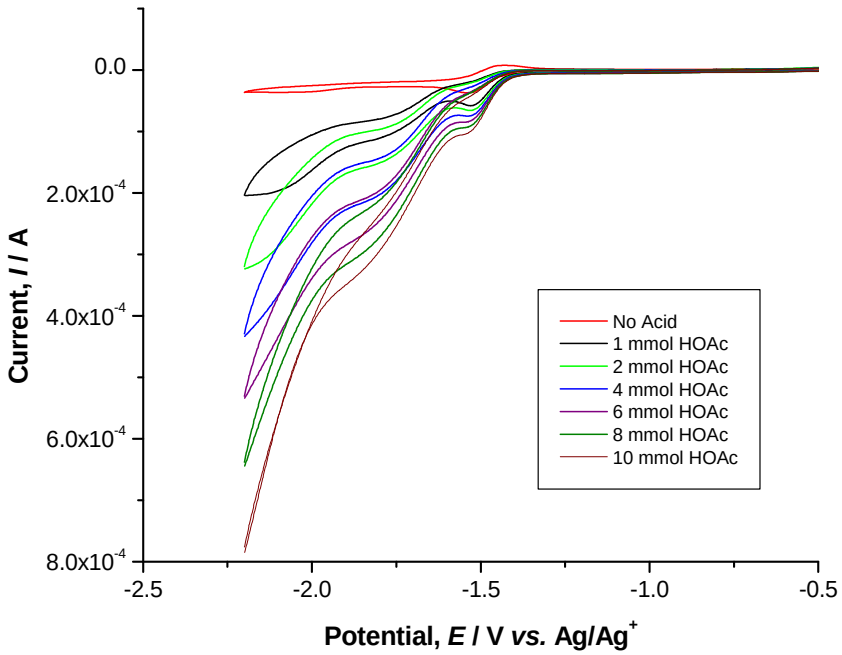

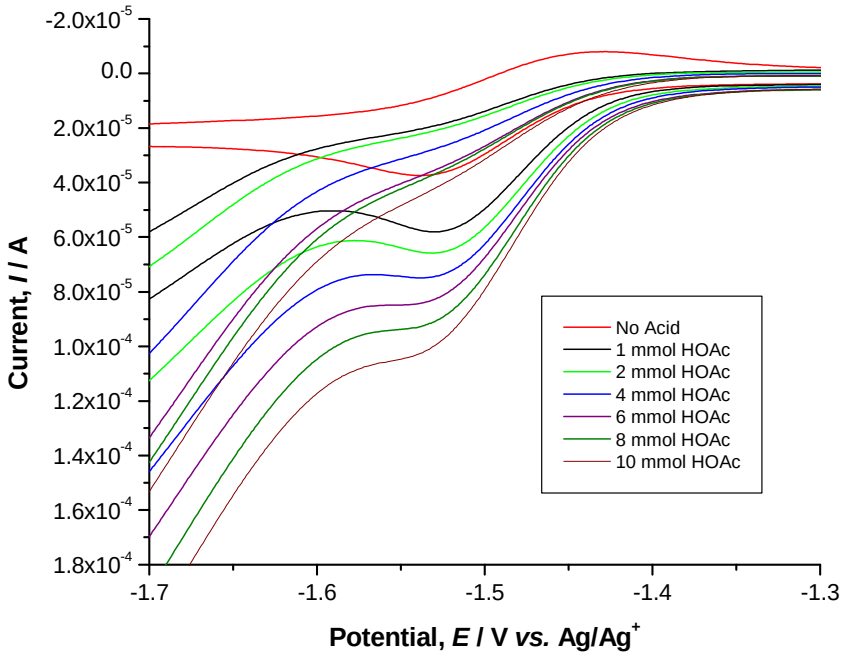

Figure 6.14: *Cyclic voltammetry of **1** [1 mM], at a GC working electrode (3 mm geometrical diameter), with HOAc (0-10 mmol) using 0.05M $TBAPF_6$ in acetonitrile as the supporting electrolyte. Scan rate: 100 mV/s.*

The mechanism of catalytic proton reduction for the hydrogenase analogue, **1**, is not as straightforward as complexes **2** – **5**. Following addition of the first aliquot of acid to the system no positive shift in the reduction potential of the $[Fe^{I}Fe^{I}] \rightarrow [Fe^{0}Fe^{I}]$ process is observed. In acid free solution this process is quasi-reversible. In the presence of acid this wave becomes irreversible and an increase in the height of the wave is observed, Figure 6.14. The current intensity continues to increase slightly with each increment of acid thereafter however these changes in current intensity are minimal. From these observations it is proposed that the first step in the reaction pathway is that of an electrochemical reduction and not a protonation of the diiron active site, Scheme 6.2

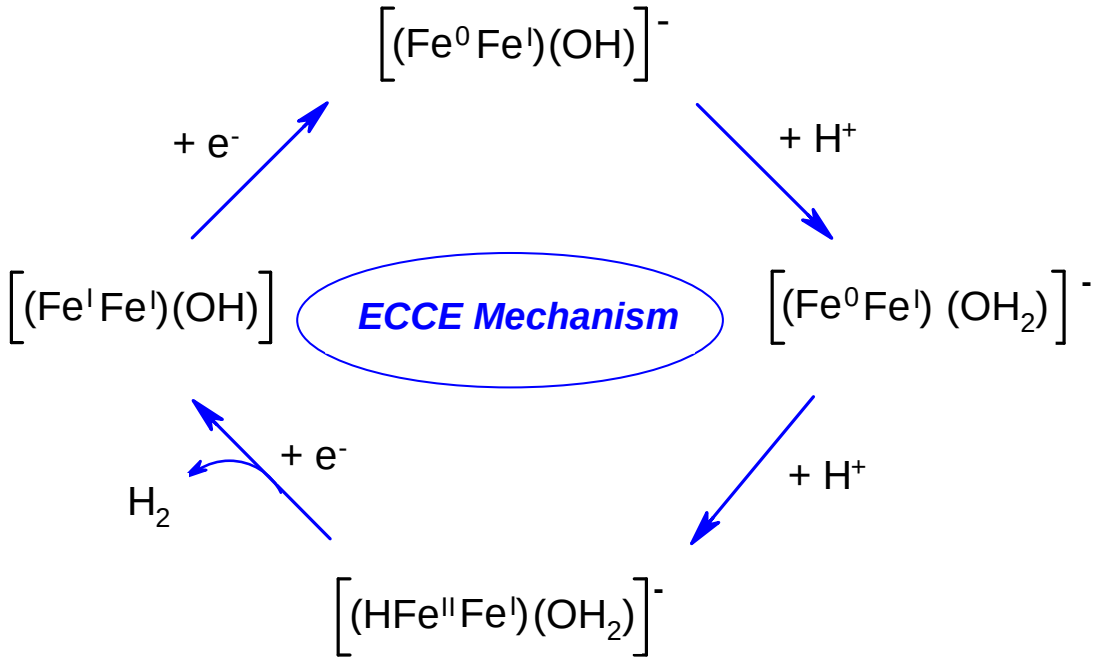

Scheme 6.2.

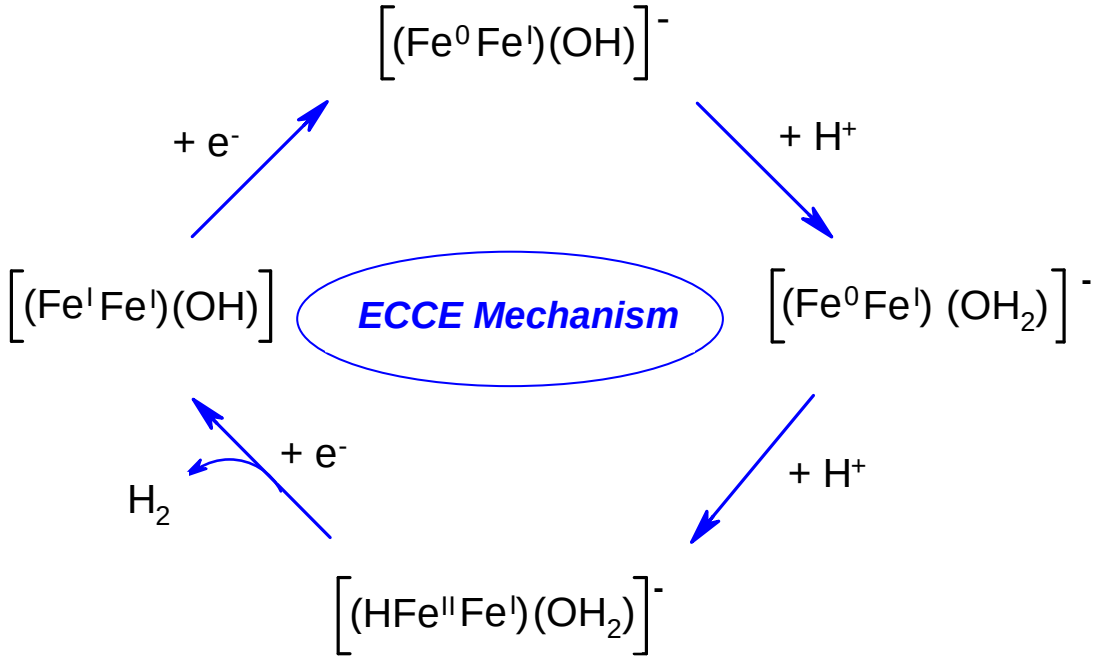

Scheme 6.2: *Proposed ECCE mechanism for the electrocatalysis incorporating hexacarbonyl diiron dithiolate complex* ***1***.

The second step of the catalytic pathway to hydrogen evolution is thought to be protonation of this singly reduced species creating the hydride species as indicated by the appearance of a new cathodic wave at approximately -1.8 V (*vs.* Ag/Ag^{+}) which is 300 mV more positive than the reduction potential of the second cathodic process in acid free solution. This process is not observed in the absence of acid. It may also be possible that the –OH group bonded to the pdt bridge, following the first reduction, acts as a proton relay between this and the diiron active site allowing the first protonation to occur at this basic site. The height of this wave increases with increasing amounts of acid added which would suggest that the electrocatalytic proton reduction is mediated from this point; the $[(\eta\text{-}H)Fe^{II}\text{-}Fe^{I}]$ intermediate complex (or alternatively the $[(OH_2)Fe^{0}Fe^{I}]$ complex. The intermediate is again protonated and upon further reduction of this protonated complex the compound finally releases H_2. An electrochemical-chemical-chemical-electrochemical (ECCE, Scheme 6.2) mechanism is proposed for the catalytic activity of **1**

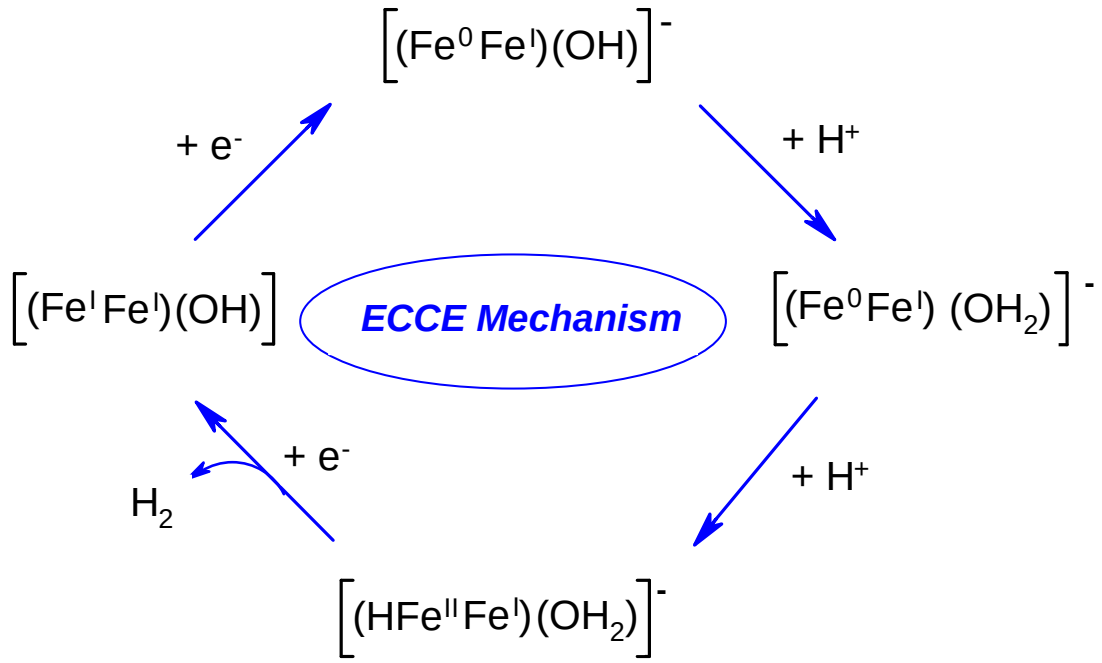

Scheme 6.2.

6.2.2 Sila-Substituted Hexacarbonyl Diiron Hydrogenase Analogues

As mentioned above, the [FeFe] hydrogenase enzyme is an efficient generator of molecular hydrogen from the reduction of protons. Mimicking the kinetic and thermodynamic properties of the enzyme is not straightforward. Problems such as high reduction potentials, lack of basicity and slow turnover rates are some of the problems arising to date with the hydrogenase analogues that have been reported.[5, 11a] A series of model compounds for the diiron hydrogenase have been synthesised where the carbon of the pdt bridge is replaced by a silicon, Figure 6.15. These include hexacarbonyl [μ-(2,2-dimethyl-2-sila-1,3-propandithiolato(2-)-*S,S'*)] diiron (**6**), hexacarbonyl [μ-(2,2-tetramethylen-2-sila-1,3-propandithiolato(2-)-*S,S'*)] diiron (**7**), hexacarbonyl [μ-(2,2-pentamethylen-2-sila-1,3-propandithiolato(2-)-*S,S'*)] diiron (**8**), dodecacarbonyl bis[μ, μ'-{2,2-bis(mercaptomethyl)-2-sila-1,3-propandithiolato(4-)-*S,S',S",S"'}*] tetrairon (**9**) and octacacarbonyl bis[μ, μ'-{2,-(mercaptomethyl)-2-methyl-2-sila-1,3-propandithiolato(3-)-*S,S',S"}*] tetrairon (**10**). The effect of the sila-substitution on the electrochemical properties of the five complexes and related analogues are discussed. The catalytic activity of each compound with respect to hydrogen production is also examined in the presence of a weak acid.

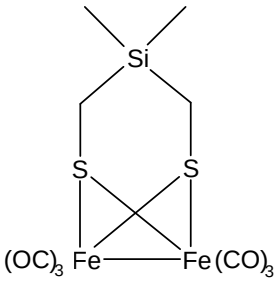

6

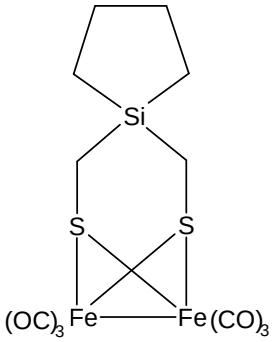

7

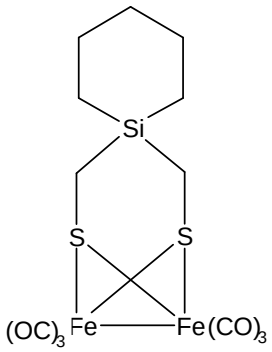

8

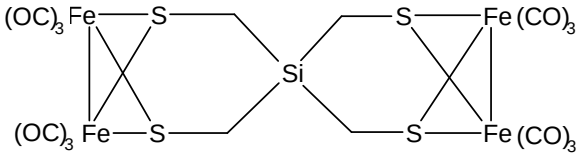

9

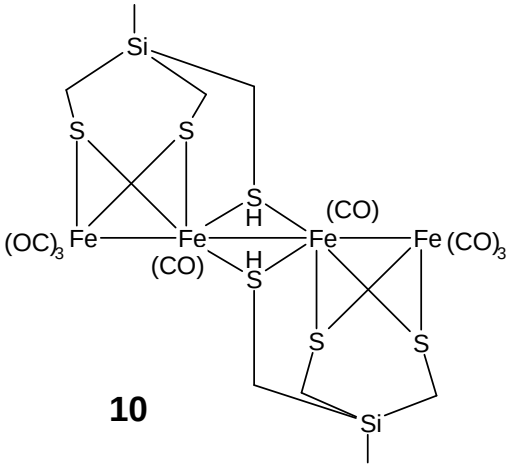

10

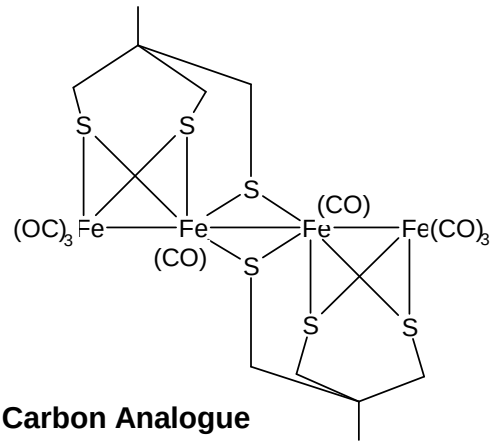

Carbon Analogue

11

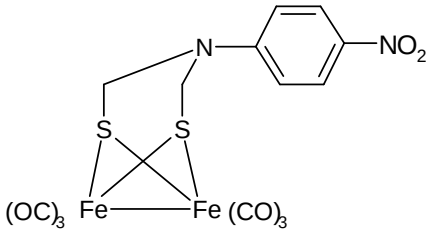

Nitro-functionalised Azadithiolate

12

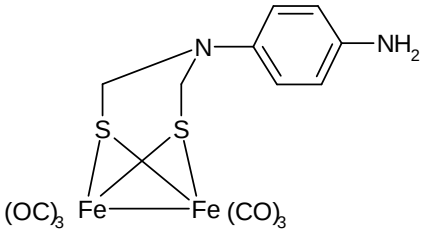

Amino-functionalised Azadithiolate

13

Figure 6.15: *Molecular structures of the sila-substituted hexacarbonyl hydrogenase analogues,* ***6 – 10****, the carbon analogue* $Fe_4[MeC(SCH_2)_3]_2(CO)_8$*,* ***11*** [17d, 28, 30] *and the nitro-* ***(12)*** *and amino-functionalised (****13****) adt derivatives* [17b] $Fe_2[(\mu\text{-}SCH_2)_2N(4\text{-}NR_2C_6H_4)](CO)_6$*, where R = H or O.*

6.2.2.1 Electrochemistry of Sila-substituted Hydrogenase Analogues

The [FeFe] hydrogenase analogues, **6** – **8** (Figure 6.15), all contain one diiron active site with the only difference between each complex found to lie in the number of methylene groups bonded to the sila-substituted dithiolate bridge.

Compound	$Fe^{I}Fe^{I}/Fe^{II}Fe^{I}$ ***[V]***	$Fe^{I}Fe^{I}/Fe^{0}Fe^{I}$ ***[V]***	$Fe^{0}Fe^{I}/Fe^{0}Fe^{0}$ ***[V]***
6	+0.79 (E_{pa})	-1.48 (E_{pc}), -1.40 (E_{pa})	-
7	+0.81 (E_{pa})	- 1.49 (E_{pc}) - 1.40 (E_{pa})	-
8	+0.81 (E_{pa})	- 1.49 (E_{pc}) - 1.39 (E_{pa})	-
9	+0.99 (E_{pa})	-1.57 (E_{pc})	-2.15 (E_{pc}) -1.89 (E_{pa})
10	+0.91 (E_{pa}) +1.04 (E_{pa})	-1.39 (E_{pc}), -1.31 (E_{pa}) -1.57 (E_{pc}), -1.46 (E_{pa})	-2.16 (E_{pc})
$[(Fe(CO)_3)_2(\mu\text{-pdt})]$ [17a, b]	+0.84 (E_{pa})	-1.57 (E_{pc}) -1.47 (E_{pa})	-2.11 (E_{pc})
Nitro-functionalized ADT Complex 12 [17b]	+0.78	-1.34 (E_{pc}) -1.28 (E_{pa})	-1.71 (E_{pc}) -1.63 (E_{pa})
Amino-functionalized ADT Complex 13 [17b]	+0.80	-1.48 (E_{pc}) -1.23 (E_{pa})	-

Table 6.2: *Electrochemical data for complexes **6** – **10**, and related compounds **11** - **13**, in acetonitrile on a GC working electrode, vs. Ag/Ag^{+} reference electrode.*

Cyclic voltammetry of complex **6** reveals that there are two redox processes occurring within the complex, the oxidation and reduction potentials of which are recorded in Table 6.2. An anodic wave is observed at positive potentials representing the irreversible oxidation of the diiron active site according to the reaction, $Fe^{I}Fe^{I} \rightarrow Fe^{I}Fe^{II} + e^{-}$. This process is also observed in the cyclic voltammetry of both **7** and **8**

and the potentials recorded for each of the three complexes show minimal variation from one to the other in the range of +0.79 to +0.81 V (*vs.* Ag/Ag^{+}).

A single reversible reduction is exhibited by each of the diiron complexes. By comparison with the electrochemistry of the complexes investigated by Darensbourg *et al.* [17a], Sun *et al.* [17b] and complexes **1** – **5**, this reduction is proposed to be a one-electron process assigned to $[Fe^{I}Fe^{I}] + e^{-} \rightarrow [Fe^{0}Fe^{I}]$. Further reduction to the $[Fe^{0}Fe^{0}]$ state was not observed for complexes **6** - **8** within the potential window investigated (-2.2 to +1.1 V, *vs.* Ag/Ag^{+}), Figure 6.16. This CV details the redox processes in **6** but it is also representative of the corresponding processes in **7** and **8**. The fact that the oxidation and reduction potentials of all three diiron hydrogenase mimics are approximately identical within experimental error suggests that the number of methylene groups or likewise the addition of a ring to the dithiolate bridge has minimal effect on the electrochemistry of the complex.

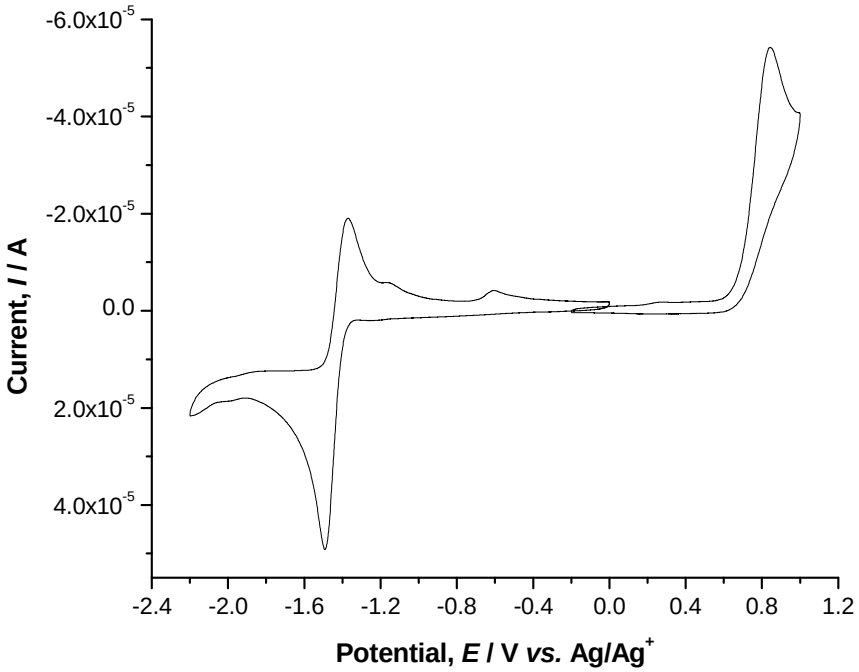

Figure 6.16: *Cyclic voltammetry of complex **6** [1mM], at a GC working electrode (3 mm geometrical diameter), in acetonitrile with 0.05 M $TBAPF_6$ as the supporting electrolyte. Scan rate: 100 mV/s.*

When comparing with the carbon based pdt bridged analogue **4**, Figure 6.10, it seems that the silicon based compounds are easier to oxidize exhibiting oxidation potentials approximately 100 mV less positive than that of **4**. Surprisingly the reduction waves show that **6 - 8** are also easier to reduce by a similar amount. Simply considering these observations in terms of electron density around the metal centre alone, a less positive oxidation potential would suggest that electron density at the Fe centre has increased arising from an increase in the electron donating ability of silicon compared to carbon. However, if this is so then it would not explain why the reduction is also a more facile process with positive shifts observed in the reduction potential. The resulting trend appears to be that the addition of the more electron-donating silicon atom to complexes **6 - 8** leads to more thermodynamically accessible oxidation and reduction processes – each complex is oxidised at a lower, less positive potential but the reduction also occurs at less negative potentials than the similar complexes containing carbon (**4**). Consideration of the location of the orbitals in the complex that are involved in the oxidation and reduction processes, reveals that the classically "bent" Fe-Fe bond actually houses both of these orbitals, Figure 6.9. The HOMO of the complex is thought to be located on this central Fe-Fe bond with the LUMO being its antibonding counterpart.[27] The trend in oxidation and reduction potentials observed above may be explained by the fact that an increase in electron density on the diiron centre as a consequence of the silicon atom on the dithiolate bridge may cause an increase in energy of the HOMO (making it easier to oxidize) and a decrease in the energy level of the LUMO resulting in a less negative reduction potential.

Where the hydrogenase models, **6** – **8** have one active site for the binding of protons and production of H_2, complexes **9** and **10** (Figure 6.15) have four Fe centres and are therefore presumed to have two active sites for binding. However, the distances between the two diiron sites in each complex are not the same and their electrochemical properties are remarkably different as a result. In the cyclic voltammetry of compound **9** one irreversible anodic wave is observed representing the oxidation of the Fe^{I} centre to Fe^{II}. Although there are two diiron active sites in the complex only one anodic wave is observed suggesting that the oxidation of each active site occurs simultaneously and therefore this wave represents two one-electron processes.[17a] Figure 6.17 illustrates this by comparing the anodic oxidative waves obtained for the tetra-iron compound **9** with the diiron single active site compound **8**.

The area under the wave for the latter (6.61 x 10^{-5} C) is approximately half that observed for **9** (1.21 x 10^{-4} C) suggesting that there are two electrons involved in this oxidative process when two diiron active sites are present in the one complex.

When scanning to negative potentials with complex **9**, one irreversible reduction is observed representing two one-electron processes corresponding to the $[Fe^{I}Fe^{I}] + e^{-} \rightarrow [Fe^{0}Fe^{I}]$ process for each diiron centre (E_{pc} = -1.05 V, *vs.* Ag/Ag^{+}). Comparing this reduction potential with that of the single active site complexes **6** – **8** (Figure 6.15) it is noted that this process experiences a positive shift of approximately 440 mV compared to the corresponding processes in the latter. A possible explanation for this lies in the fact that there is only one silicon atom in this complex which is bridged between the two diiron centres. As a result of this "sharing" of the silicon atom between the two active sites there is less additional electron density around the metal centres of each and therefore it is easier to reduce to the $[Fe^{0}Fe^{I}]$ state.

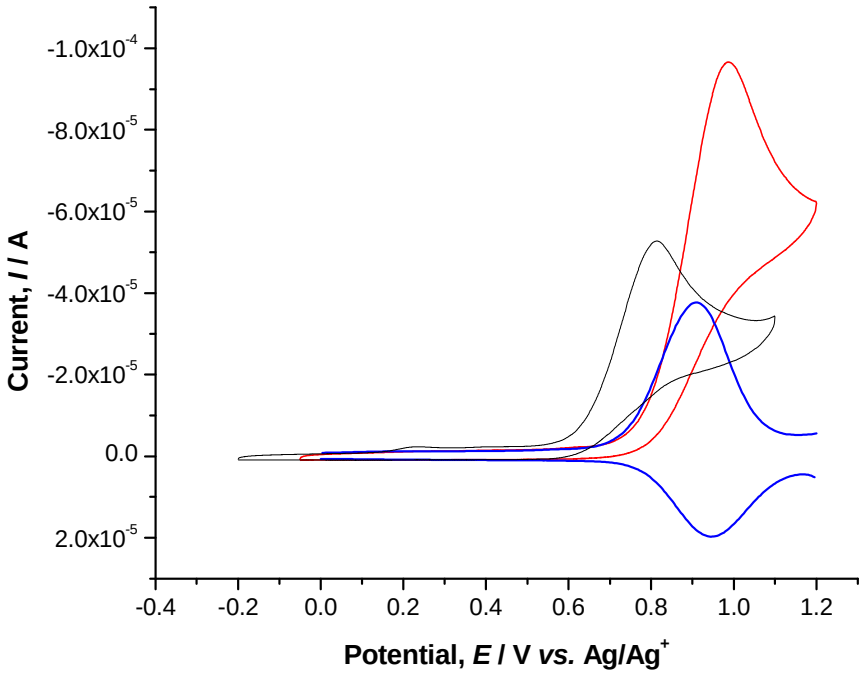

Figure 6.17: *Cyclic voltammetry of compounds **8** (black line) [1 mM] and **9** (red line) [1 mM] and differential pulse analysis of **9** (blue lines) at a glassy carbon electrode (3 mm geometrical diameter), in acetonitrile with 0.05 M $TBAPF_6$ as the supporting electrolyte. Scan rate: 100 mV/s.*

The analysis of the oxidation and reduction processes in complex **9** leads to a conclusion that little or no interaction exists between the two diiron active sites and the silicon bridge acts as a poor mediator for communication between the two. Where communication exists in the mixed valence state two separate redox waves would be expected for each process.[31] This is also observed in the tri-active site complex **5** (Figure 6.10) where a single anodic wave is observed representing the simultaneous oxidation of the diiron active sites.

Marked differences are noted between the electrochemistry of complex **9** and that of the second tetra-iron complex, **10**. In the latter a [4Fe6S] cluster exists comprised of two [2Fe2S] clusters that are connected via two bridging thiol groups. The length of the bond between the inner two Fe atoms is shorter than that of the bond length between the two Fe atoms of each diiron active site. The structure of **10** is very similar to that of a tetra-iron hydrogenase mimic reported by Pickett *et al.* [28] with the most obvious difference being that the central atom of the dithiolate bridge is a carbon in the Pickett complex as opposed to a silicon atom in complex **10**. The molecule is arranged around a centre of symmetry with the central unit being that of the planar dithiolate bridged diiron unit. Picket *et al.* proposed an $[Fe^{I}Fe^{II}Fe^{II}Fe^{I}]$ assembly for the carbon analogue of **10** where electrocatalytic proton reduction occurs from the unique all Fe^{I} state.[17d] However, electrochemical results obtained for the sila-substituted **10** suggest otherwise and therefore the assignment of the oxidation states of each Fe atom within this structure differ from that reported for the carbon analogue.

The cyclic voltammogram and the differential pulse data recorded for **10** (Figure 6.18) show reduction potentials in the region of the commonly discussed $[Fe^{I}Fe^{I}] + e^{-} \rightarrow [Fe^{0}Fe^{I}]$ reduction step in [2Fe2S] complexes.[17a & b, 32] The diiron hydrogenase analogues **6** – **8** contain a single diiron active site. In these complexes both iron centres are thought to be in the Fe^{I} oxidation state. This is verified by Mössbauer spectroscopy, *vide infra*. Given that the reduction potentials of **10** are within the range of those recorded for the single active site complexes (Table 6.2) and also the fact that the Pickett carbon complex (Figure 6.15) is reduced at potentials approximately 140 mV more positive than this silicon analogue (*vide infra*, Table 6.3) it is suggested that the compound does not contain an $[Fe^{I}Fe^{II}\text{-}Fe^{II}Fe^{I}]$ assembly as described by Picket *et al.* [17d]. Instead the data indicates the presence of two $[Fe^{I}Fe^{I}]$ dinuclear units which are

connected via two thiol-groups. The assignment of this charge to the iron centres and the presence of thiol groups bridging the two diiron active sites is confirmed with further experiments, *vide infra*.

The cathodic waves at –1.38 and –1.57 V are therefore assigned to quasi-reversible reductions according to the following equations

$$[Fe^{I}Fe^{I\cdots}Fe^{I}Fe^{I} + e^{-} \rightarrow Fe^{I}Fe^{0\cdots}Fe^{I}Fe^{I}] \qquad -1.38\ V$$

and

$$[Fe^{I}Fe^{0\cdots}Fe^{I}Fe^{I} + e^{-} \rightarrow Fe^{I}Fe^{0\cdots}Fe^{0}Fe^{I}] \qquad -1.57\ V$$

which is in contrast to the reported carbon derivative. A third reversible reduction is noted at more negative potentials (E_{pc} –2.16 V). This may be assigned to the further reduction of the diiron active sites to the $[Fe^{0}Fe^{0}]$ oxidation state.

The compound shows two closely spaced irreversible positive processes, Figure 6.18, assigned as the oxidation of both diiron active sites according to the following scheme: $[Fe^{I}Fe^{I} \rightarrow Fe^{I}Fe^{II} + e^{-}]$. The presence of two separate anodic peaks may be due to the different coordination environment of the redox active sites: it is difficult to say whether the first oxidation occurs on the inner Fe-Fe bond that bridges the two active sites or whether it is located on the outer metal-metal bond of one of the active sites. The Fe atoms of the inner diiron bond are each coordinated to a single carbonyl ligand as well as two bridging sulphur atoms which are possibly protonated, *vide infra*, whereas the coordination environment of the outer Fe atoms is different given that they are each coordinated to three carbonyl ligands as well as the bridging sulphur atoms. The separation between the anodic waves may also indicate interaction across the dithiol bridge between the two active sites.

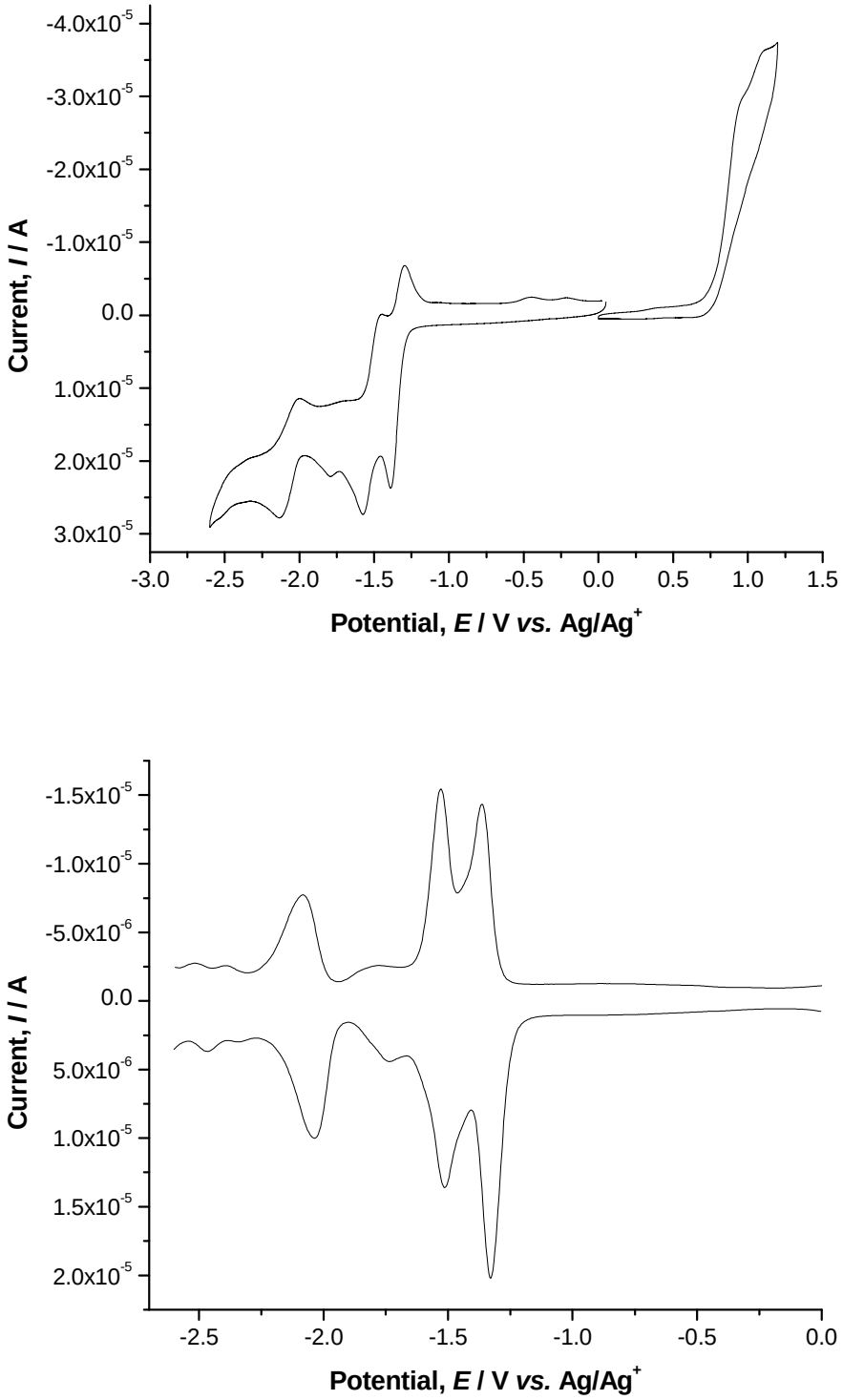

Figure 6.18: *Cyclic voltammetry (top) and differential pulse voltammetry (bottom) of complex **10** [1 mM] at a glassy carbon electrode (3 mm geometrical diameter), in acetonitrile with 0.05 M $TBAPF_6$ as the supporting electrolyte. Scan rate: 100 mV/s.*

The reduction potentials reported by Pickett *et al.* for the carbon derivative [28] were recorded using dichloromethane as the electrochemical solvent and a Ag/AgCl electrode as the reference electrode. Two separate cathodic waves are observed for this carbon compound, separated by approximately 370 mV. The first wave is assigned to the $[Fe^{I}Fe^{II}Fe^{II}Fe^{I}] + e^{-} \rightarrow [Fe^{I}Fe^{I}Fe^{II}Fe^{I}]$ process with addition of the second electron leading to the all Fe^{I} state. This large difference between the two reduction potentials, while not conclusively, can be an indication of communication between the redox sites within the complex following the initial reduction. Interaction occurring suggests that the locations of the reductive sites are not insulated within the molecule thereby possessing the ability to interact with one another. Pickett *et al.* [28] propose that the first reduction results in the addition of an electron to the central Fe-Fe antibonding orbital. This anionic species is stable and fully reversible as verified by spectroelectrochemistry.[17d] Addition of the second electron to this orbital is a quasi-reversible process; the dianion is relatively unstable if the duration of this second reduction step is longer than 10 seconds and a concerted cleavage of this central diiron bond results leading to the formation of a mixture of decomposition products.[17d] The electrochemistry of **10** was also recorded under these conditions to ensure an unambiguous comparison between the two compounds, Table 6.3. The first reduction wave of the carbon analogue occurs at a potential that is approximately 140 mV more positive than that of the corresponding process in compound **10**. A difference of 50 mV is noted for the second reduction potential.

	E_{pa} [V] $Fe^{I}Fe^{I}/Fe^{II}Fe^{I}$	$E_{½}$ [V] $Fe^{II}Fe^{I}/Fe^{I}Fe^{I}$	$E_{½}$ [V] $Fe^{I}Fe^{I}/Fe^{0}Fe^{I}$	E_{pc} [V] $Fe^{I}Fe^{0}/Fe^{0}Fe^{0}$
10 (CH_3CN)	+0.91	-	-1.35	-2.16
	+1.04		-1.52	
10 (CH_2Cl_2)	+1.12	-	-1.25	-1.54
			-1.43	
Carbon Analogue (CH_2Cl_2) [17d, 28]	-	-1.02 -1.39	-	-

Table 6.3: *Electrochemical data for complex **10** and the carbon analogue, in acetonitrile and dichloromethane. All values have been corrected against the Ag/Ag^{+} reference electrode using the Fc/Fc^{+} couple as the internal standard.*

The redox processes of these iron hydrogenase models are clearly solvent dependent, with negative shifts of approximately 100 mV observed when changing from dichloromethane to acetonitrile. An ill-defined oxidation is observed at a more positive potential than the corresponding process in acetonitrile for complex **10**. This wave is not associated with oxidation of the solvent since in blank electrolyte no such process is observed. The third reductive process observed in acetonitrile is not observed in dichloromethane due to solvent cut-off.

Table 6.3 clearly outlines the differences between the electrochemistry of complex **10** with that of the carbon analogue. The results obtained for **10** do not support the existence of an $[Fe^{I}Fe^{II}Fe^{II}Fe^{I}]$ arrangement suggesting differences in the coordination environments and oxidation states of the Fe atoms in complex **10**. To further investigate the possibility of an all Fe^{I} arrangement in the tetra-iron complex **10** Raman, Mössbauer and susceptibility experiments were carried out.

Professor Coey, of Trinity College Dublin, investigated the redox states of the Fe centres through Mössbauer and susceptibility measurements. The results obtained for **10** were compared with the diiron complex **6** (Figure 6.15) which is taken as a well-established example of a compound with an $Fe^{I}Fe^{I}$ cluster. The Mössbauer spectra were fitted by the standard least-squares minimization procedure. The spectrum for **6** shows a quadrupole doublet with an isomer shift of $\delta = -0.04 \pm 0.02$ mm s^{-1} relative to α_{Fe} and a quadrupole splitting $\Delta = 0.78 \pm 0.02$ mm s^{-1} (Table 6.4, Figure 6.19). These values are in agreement with those obtained by Song and co-workers [23d] of $\delta = -0.02$ mm s^{-1} and $\Delta = 0.81$ mm s^{-1} for a similar dinuclear compound. The asymmetry of the spectrum indicates the presence of some of the iron (~ 35 %) in a second site giving a doublet with broadened lines and $\delta = 0.19 \pm 0.02$ mm s^{-1} and $\Delta = 0.52 \pm 0.02$ mm s^{-1}. Susceptibility measurements on this compound in the liquid helium temperature range show that less than 1% of the iron in the sample has an unpaired spin. Hence any unpaired electrons in the low spin Fe^{I} centres are paired to form a covalent bond in the dinuclear complex. Since the covalent bond length expected for an $Fe^{I}Fe^{I}$ bond is 233 pm the X-ray Fe-Fe distance of 252 pm is in agreement with this interpretation. The iron in the minority site appears to be low-spin Fe^{II}, which is quite consistent with the observed isomer shift.

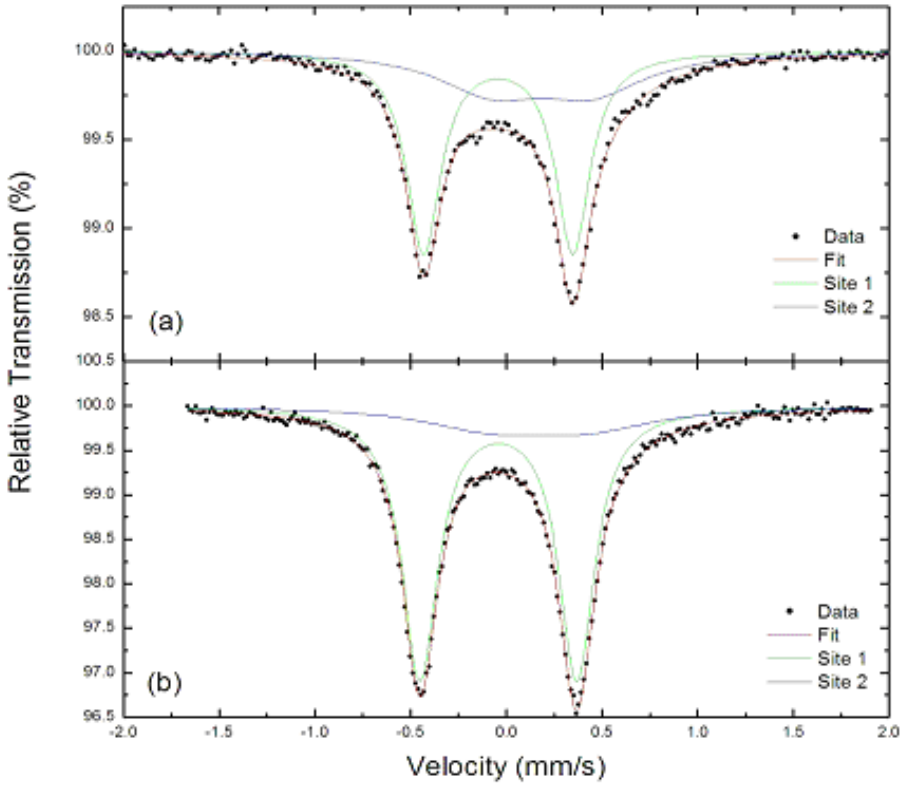

Figure 6.19: *Room-temperature Mössbauer spectra for compounds **6** and **10**. The fit parameters for the quadruple doublets are shown in Table 6.4 below.*

Sample	***Isomer shift mm s^{-1}***	***Quadrupole splitting mm s^{-1}***	***Linewidth mm s^{-1}***	***Relative Area %***
6	-0.04 (2)	0.78 (2)	0.11 (1)	63
	0.19 (2)	0.52 (2)	0.34	37
10	-0.04 (2)	0.82 (2)	0.11 (1)	93
	0.17 (4)	0.51 (4)	0.42 (4)	7

Table 6.4: *Room temperature Mössbauer data for compounds **6** and **10**.*

The Mössbauer spectrum for compound **10** is similar (Figure 6.19, Table 6.4). The main doublet has an isomer shift δ = -0.04 $\pm$ 0.02 mm s^{-1} and a quadruple splitting Δ = 0.82 $\pm$ 0.02 mm s^{-1}. The minority site (~ 7 % of the iron) gives a doublet with

broadened lines and $\delta = 0.17 \pm 0.04$ mm s^{-1} and $\Delta = 0.51 \pm 0.04$ mm s^{-1}. The Curie-law susceptibility data in this case is consistent with 8% of the Fe atoms possessing a spin of ½, or 1% of the Fe being present as high-spin Fe^{II} (Figure 6.20). It is surprising that the different coordination sphere of the outer and inner Fe atoms does not lead to any significant difference in the quadruple splitting.

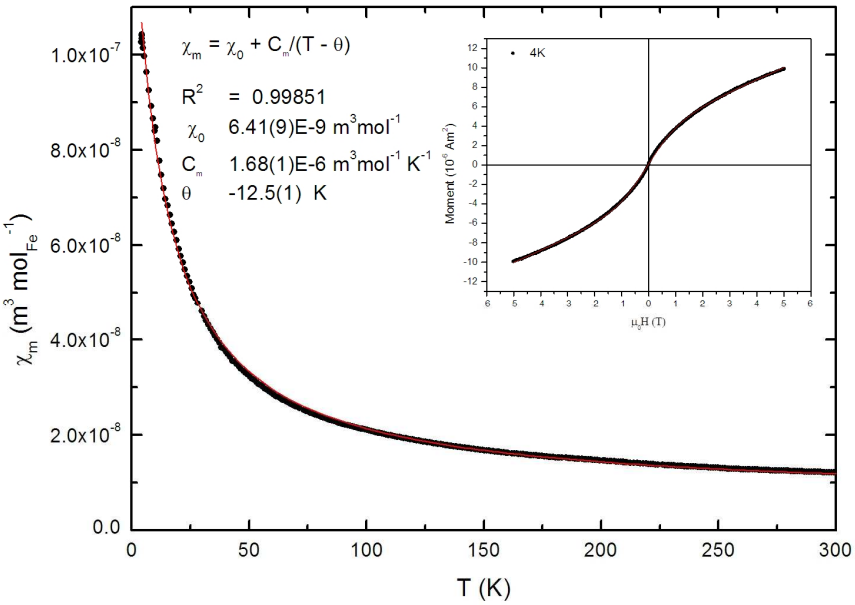

Figure 6.20: *Scan of the magnetization of sample **10**, measured in an applied field of 800 kA m^{-1}. The data are fitted to a law of the form $\chi = \chi_0 + C/(T-\theta)$ where χ_0 is a small temperature-independent term. The Curie constant C is used to deduce the presence of unpaired spins, using the result $C = 1.57\ 10^{-6}\ 4S(S+1)$ per mole of ions with spin S.*

If an all Fe^{I} arrangement is present in the tetra-iron complex **10** then, in order to balance the charges within the compound, the two central sulphur atoms must be protonated. This was investigated using Raman spectroscopy carried out by Professor Tacke in the University of Würzburg, Germany. Figure 6.21 shows the Raman spectrum of **10**, measured with an excitation wavelength of 633 nm. The spectrum is dominated by methyl and methylene group vibrations, e. g. the strong C-H stretching vibration at 2914 cm^{-1}, the C-S and C-Si stretching vibrations at 701 cm^{-1}, different

CH_3 and CH_2 deformation modes at 1606 and 980 cm^{-1} and the Fe-S stretching vibrations at 513 cm^{-1}. The signal at 2593 cm^{-1} is assigned to an S-H-stretching mode. In this spectral region, no other vibrational frequencies occur. The signal is therefore a very strong indicator of the existence of SH moieties in **10**.

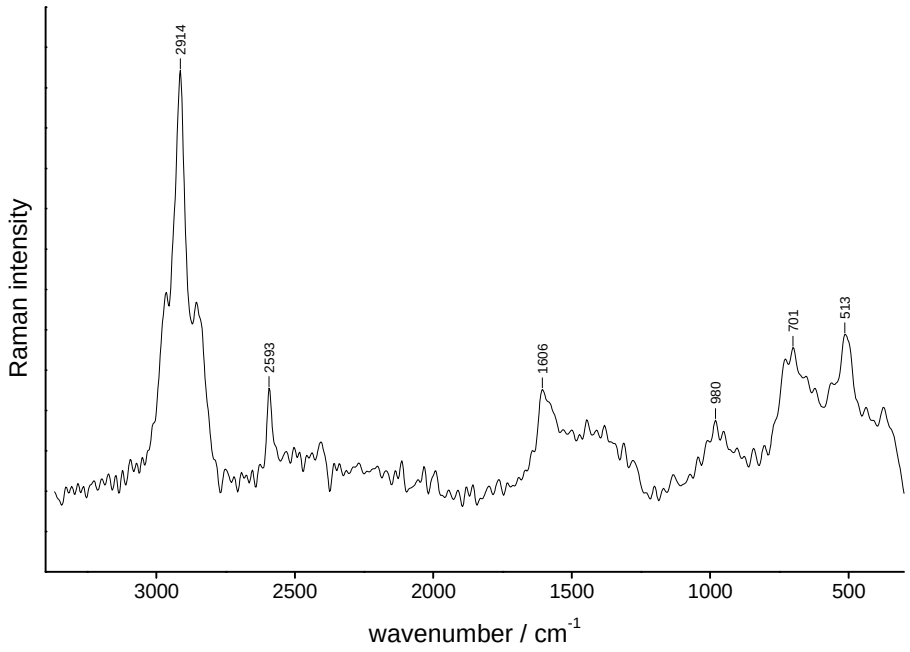

Figure 6.21: *Raman spectrum of compound **10** showing the S-H vibration at 2593 cm^{-1}.*

These results and in particular the similarity of the data observed for samples **6** and **10** do not provide any evidence to suggest that half the iron in compound **10** is present in Fe^{II} centres. Based on these results, together with the electrochemical data an alternative structure is proposed where all four centres are in the Fe^{I} state and the two central sulphur atoms are present as thiol groupings, Figure 6.15.

6.2.2.2 Electrocatalytic Proton Reduction of Sila-substituted Hydrogenase Analogues

The potential of each of the five sila-substituted hydrogenase models to act as catalysts in the reduction of protons to hydrogen was investigated by analysing their cathodic electrochemistry in the presence of a weak acid, HOAc (1–10 mmol) in

acetonitrile. The three diiron compounds, **6** – **8** all exhibit similar catalytic properties again emphasizing that the number of methylene groups bonded to the silicon atom of the bridge bears minimal effect on the activity of the complex. In contrast to complexes **1 – 5** a positive shift of approximately 60 mV (to -1.34 V, *vs.* Ag/Ag^{+}) is observed for the first (least negative) cathodic process upon addition of 1 mmol of acid, Figure 6.22. A loss in the reversibility of this peak is also observed which is common for hydrogenase models in acidic environments due to the rapid formation of hydride intermediates.[6d & f, 17a & b] In addition a second irreversible process is observed at the more negative potential of -1.82 V, *vs.* Ag/Ag^{+}. This process is absent from the CV in acid-free solution, Figure 6.16, and the current of this second process increases with each increment of acid added thereafter. The reduction potential of this cathodic process also shifts to more negative potentials as the concentration of acid increases – a consequence of an electrochemical catalytic process.[29]

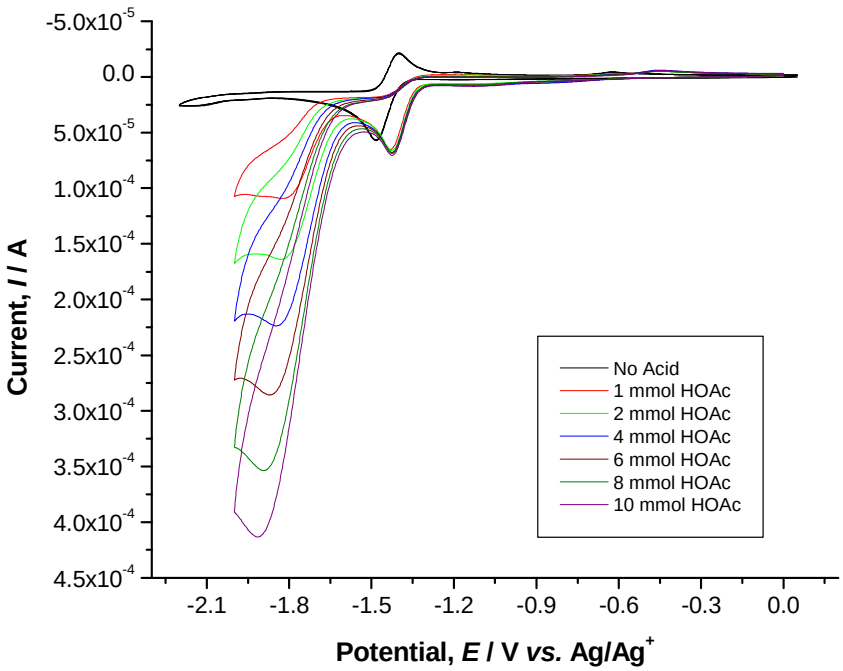

Figure 6.22: *Cyclic voltammetry of **6** [1 mM] with HOAc (0-10 mmol) in acetonitrile. Scan rate: 100 mV/s.*

Upon addition of 1 mmol of acid, the reduction potential of the first peak in the cyclic voltammetry of complexes **7** and **8** was shifted in the positive direction by

approximately 50 and 60 mV respectively, together with an increase in the current intensity. This increase in current was only observed when the concentration of acid was 1 mmol and no further increase was observed with each increment of acid added thereafter. A second reduction wave was observed at more negative potentials in acidic solution, the current intensity of which exhibits an increase with each aliquot of acid added to the solution indicating the occurrence of the catalytic process.

Following addition of acid to the tetra-iron complex **9**, shifts are noted for each of the reduction waves. The first of the cathodic peaks representing $[Fe^{I}Fe^{I}] + e^{-} \rightarrow [Fe^{0}Fe^{I}]$ exhibits a shift of approximately 160 mV in the negative direction and the wave appears to split into two waves (E_{pc} = -1.20 and -1.36 V) when the concentration of acid in solution is 1 mmol. These two waves appear to merge again when the concentration of acid is 4 mmol and above. This may occur as a result of a change in the coordination sphere of one of the diiron centres and in sufficient acid concentration the coordination spheres of each diiron active site are again identical. The second reduction wave corresponding to the $[Fe^{0}Fe^{I}] + e^{-} \rightarrow [Fe^{0}Fe^{0}]$ process is shifted initially by approximately 200 mV to a more positive potential. This shift is decreasing with each increment of acid added. Both waves experience an increase in current intensity upon addition of 1 mmol acid with this rise continuing for the second of these peaks as the concentration of acid increases, Figure 6.23.

The electrocatalytic properties of the second tetra-iron compound **10** toward hydrogen production were also investigated in the presence of the weak acid. Upon addition of acid the reduction potentials of the first two reduction peaks were shifted to more positive potentials by 15 and 120 mV for the first and second reduction processes, respectively. The thermodynamic effect on the second reduction potential is far greater than that of the first wave. Addition of the first electron to one of the diiron active sites leads to an increase in the distance between the two active sites and the resulting change in electron density leads to a more basic second site and a higher susceptibility towards protonation prior to addition of the second electron is observed. The current intensity of this second wave exhibits a gradual increase with each sequential increment of acid added. This may indicate that the electrocatalytic formation of hydrogen may begin from this $Fe^{0}Fe^{I}$ redox state.

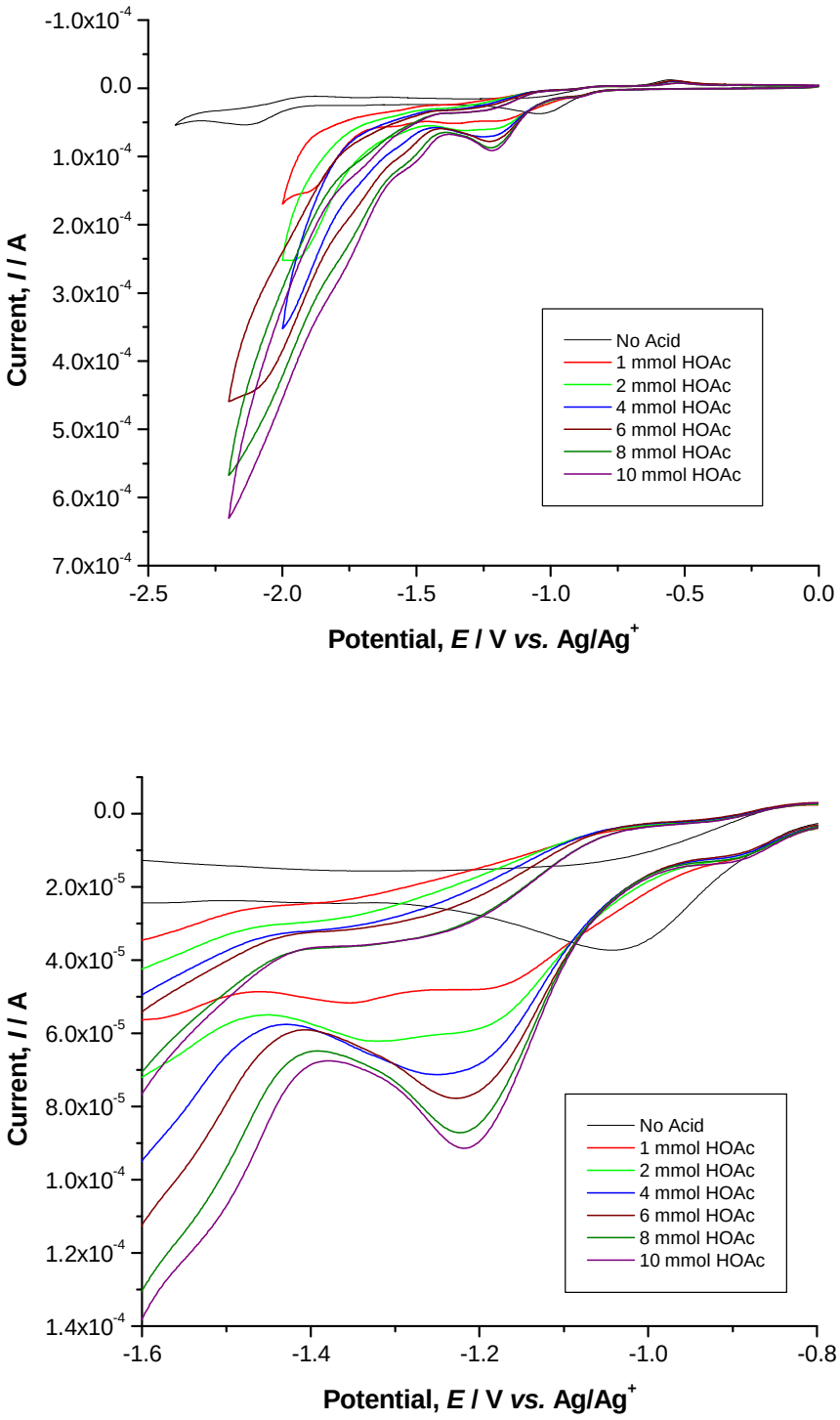

Figure 6.23: *Cyclic voltammetry of* ***9*** *[1 mM] with HOAc (0-10 mmol) in acetonitrile (top) with focus on the potential region of -1.6 to -0.8 V (bottom). Scan rate: 100 mV/s.*

However, as observed for **6** - **8**, large currents are found in the region of ~ –1.8 V with increasing intensity for growing acid concentration. When complex **10** was analysed in dichloromethane this new wave (approximate E_{pc} = -1.6 V, *vs.* Ag/AgCl, in acidic solution) is not observed in acid free solution as it falls outside the potential window of this particular electrochemical solvent, Figure 6.24. In acetonitrile this wave experiences a positive shift of approximately 170 mV. This shift in potential may suggest further protonation to the complex when in the $[Fe^{I}Fe^{0}Fe^{I}Fe^{0}]$ state. The electrocatalytic currents are much stronger than those observed for the second reduction wave suggesting that hydrogen production from an $Fe^{0}Fe^{0}$ diiron active site may be a more efficient producer of hydrogen from reduction of protons.

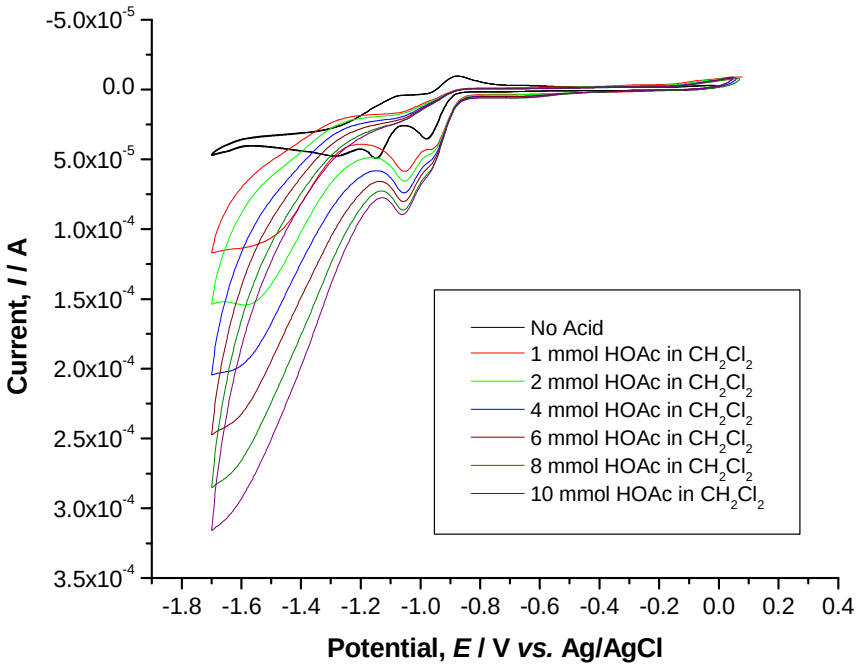

Figure 6.24: *Cyclic voltammetry of **10** [1 mM] with HOAc (0-10 mmol) in dichloromethane.*

Upon addition of acid to the diiron hydrogenase analogues, **6**, **7** and **8** and to the tetra-iron model, **10**, a positive shift in the potential of the first reduction wave is observed. This would suggest that the first step in the electrocatalytic mechanism is a chemical process involving protonation at a basic site on each complex. Related functionalized diiron azadithiolate compounds reported in the literature [17b] (Figure 6.15) also show a

shift in the positive direction upon addition of acid. The nitrogen atom on the dithiolate bridge is a basic site and readily accepts a proton in acidic solution which creates this shift. The protonated complex is then reduced and following a second protonation step, hydrogen is evolved, mediated from the $[(HFe^{II}Fe^{I})(NH)]^{+}$ redox state with a CECE mechanism proposed.

At first glance of complexes **6** – **8** and **10** there appears to be an absence of any basic sites where this initial protonation step may occur. No mechanism reported to date can explain this positive shift in the first reduction potential.[23d, 33] A possible alternative mechanism may be proposed where the initiation step in the catalytic pathway can be the protonation of one of the sulphur atoms of the dithiolate bridge. There is currently little or no evidence of the protonation of coordinated sulphur being involved in the electrocatalytic evolution of hydrogen from reported [FeFe] hydrogenase models. However, Glass *et al.* [34] have shown, using density functional theory (DFT) calculations and photoelectron spectroscopy, that for tin containing compounds the σ(Sn-C) orbital interacts with a 3p(S) orbital. These inductive and hyper-conjugative interactions increase the electron density on the sulphur atom. As a direct result of this the basicity of the sulphur atom increases. Silicon, also a group IV element may induce the same effect on the sulphur atom as that observed with tin. Considering this inductive effect, and taking into account the electrochemical results, a CECE mechanism is proposed for the diiron complexes **6** – **8** and the tetra-iron compound **10**, Scheme 6.3.

Upon addition of acid the initial $[Fe^{I}Fe^{I}]$ species is protonated with the basic site being a sulphur atom of the dithiolate bridge. Reduction of this protonated species leads to the formation of the $[Fe^{I}Fe^{0}SH]$ intermediate with a bridging carbonyl ligand [33b] creating a free coordination site. The second protonation step in the pathway may occur here at this free coordination site resulting in the terminally bridged hydride complex, $[\eta\text{-}HFe^{II}Fe^{I}SH]^{+}$. This intermediate then undergoes further reduction back to the initial $[Fe^{I}Fe^{I}]$ compound with evolution of hydrogen.

In the tetra-iron complex **9** there is only one silicon atom which is “shared” between the two diiron active sites. As a result of this the inductive effect of the silicon [34] on the sulphur atoms of the dithiolate bridges is not as strong as that observed for the

other four complexes. Therefore the basicity of the sulphur atoms is reduced and the complex no longer possesses a basic site whereby protonation can initiate the catalytic cycle.

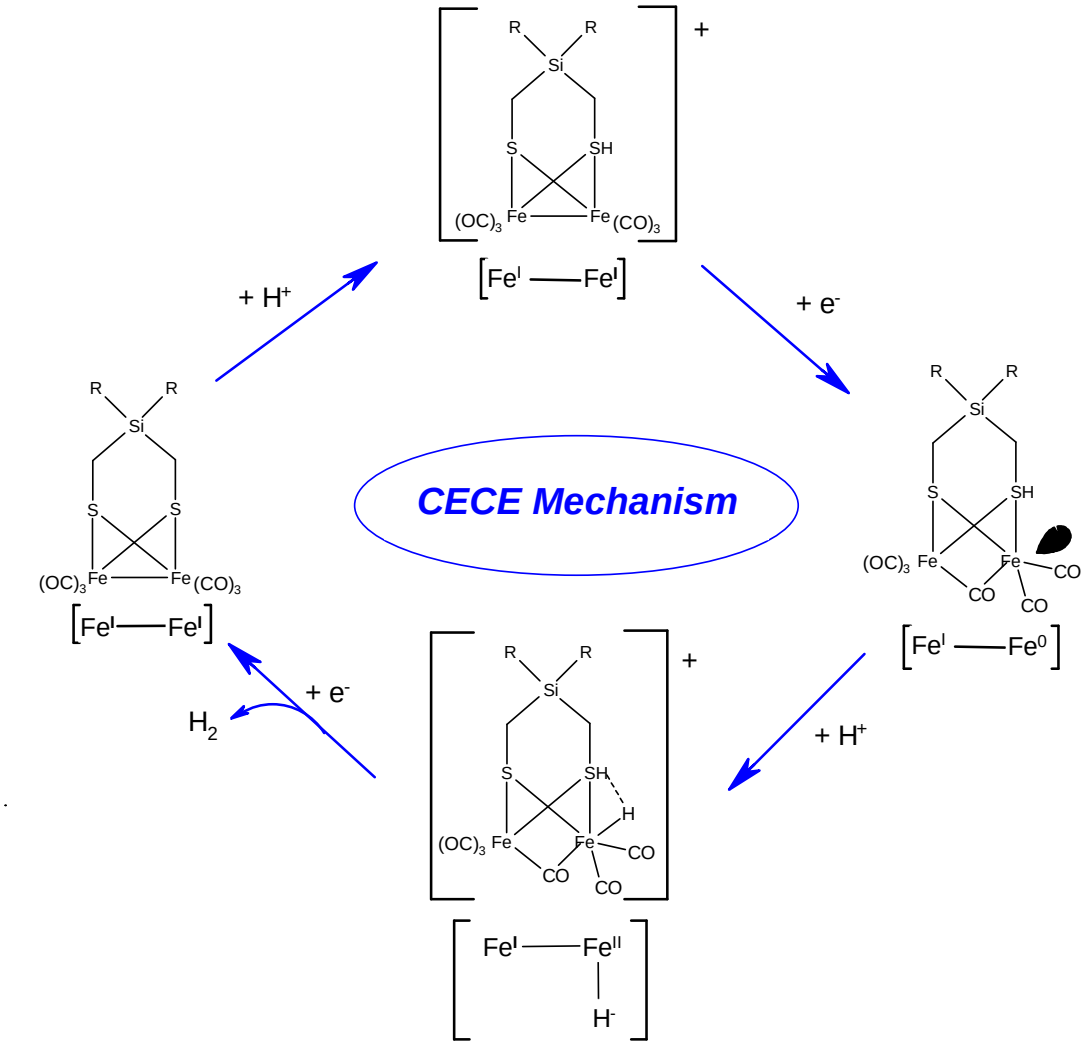

Scheme 6.3: *Proposed CECE mechanism for the electrocatalysis incorporating sila-substituted hexacarbonyl diiron dithiolate complexes* ***6*** *–* ***8*** *and* ***10*** *where the catalytic cycle is initiated by protonation of a sulphur atom of the dithiolate bridge.*

This can be seen by the negative shift observed for the first reduction process upon addition of acid to the complex. The second reductive wave does experience a positive shift in potential in acidic solution thereby suggesting the presence of a protonated intermediate. An ECEC mechanism is tentatively proposed for complex **9** where H_2 evolution is mediated from the [Fe^0Fe^0] redox state.

6.4 Conclusions

In the on-going quest to prevent further climate change and develop novel alternatives to replace the current energy sources used today, scientists have been exploring the route of using cleaner and more efficient fuels, in particular the use of hydrogen in fuel cells. Nature's hydrogenase enzymes are incredibly efficient biological microorganisms possessing the ability to produce protons from the oxidative uptake of molecular hydrogen and alternatively produce the latter from the reduction of protons (a function carried out by the [FeFe] hydrogenase enzyme). The structure of the active site of the FeFe hydrogenase bears a striking resemblance to well-known organometallic synthetic compounds of the formula $[Fe_2(CO)_6(\mu\text{-}SR)_2]$. This has led to increasing interest into the further development of synthetic models of the diiron hydrogenase active site and their properties in terms of the electrocatalytic reduction of protons to molecular hydrogen.

The electrochemistry of a series of [FeFe] hydrogenase analogues, and their ability to catalytically produce hydrogen from a low valent state using the weak acid, acetic acid, as the proton source, have been discussed in this chapter. Complexes **1** – **5** (Figure 6.10) all contain the hexacarbonyl diiron active site with different substituents on the central carbon of the propanedithiolato (pdt) bridge. The electrochemistry of all five complexes reveals one irreversible oxidation with two cathodic waves observed at negative potentials. The latter represent the quasi-reversible reduction (least negative wave) of the all Fe^I complex to the $[Fe^IFe^0]$ redox state followed by a second reduction to the lower valent all Fe^0 state. The evolution of hydrogen is mediated from this doubly reduced state forming the $[\eta\text{-}HFe^{II}\text{-}Fe^0]^-$ intermediate with subsequent protonation leading to the evolution of H_2. An electrochemical-electrochemical-chemical-chemical (EECC) mechanism is proposed for complexes **2** – **5**. Complex **1** reveals the formation of a protonated intermediate following the first reduction to the $[Fe^IFe^0]$ state and an ECEC mechanism is presented for this complex.

In contrast to the pdt bridged type complexes, **1** – **5**, the diiron hydrogenase models, **6** – **10** (Figure 6.15) all contain a silicon atom in replace of the central carbon on the dithiolate bridge as a means of investigating the influence of sila-substitution on the electrochemical properties and catalytic activity of these compounds. It is noted that

sila-substitution has a large influence on the catalytic pathway. By introducing silicon, the basicity of the sulphur atoms increase and this allows direct protonation of the bridgehead sulphur atoms as observed during cyclic voltammetry in the presence of acetic acid. The presence of the silicon atom leads to an increase in electron density around the diiron active site with consequent increases and decreases observed for the HOMO and LUMO levels of the diiron bond respectively. This is evident in the electrochemical date where compounds **6** – **8** appear to be more easily oxidised (increased energy of HOMO) and also more easily reduced (decreased energy of LUMO) than some of the pdt-bridged type analogues. The number of carbons bonded to the Si atom of the dithiolate bridge increases from complex **6** to **8**. It is noted that the ring strain and therefore increasing spatial demand has no influence on the catalytic cycle.

There are several similar features between the structure of complex **10** and that of the carbon analogue as reported by Pickett *et al.*[17d, 28] The electrochemical, Mossbauer and susceptibility features do, however, suggest an all Fe^{I} structure rather than the presence of Fe^{II} as proposed for the carbon species. This is further confirmed by the Raman spectra which indicate the presence of –SH groupings. A CECE mechanism is tentatively proposed for complexes **6** – **8** and **10** whereby the complex is protonated at the basic sulphur site of the dithiolate bridge prior to the first reduction process. This is evident in the positive shift of the first cathodic wave in acidic solution compared to the same process in acid free solution. The evolution of hydrogen transpires from the $[\eta\text{-}HFe^{II}Fe^{I}SH]^{+}$ intermediate.

The tetra-iron hydrogenase analogue, **9** does not experience this protonation of a sulphur atom upon addition of acid. Instead a negative shift in the reduction potential of the first cathodic wave is observed and as a result an ECEC mechanism is proposed. This weakening of the protonation phenomenon that is observed for **6** – **8** and **10** may be due to the different coordination modes and the "sharing" of the silicon atom between the two diiron active sites of **9**. It is also evident from the cyclic voltammetry that little or no interaction exists between the two active sites in this complex.

The chemistry of the [FeFe] hydrogenase enzyme has proven to be quite complicated. The quest to fully understand this fascinating cycle (occurring within nature a thousand times every second) is not without its difficulties because of the short lived intermediates within the cycle as a result of very high turnover rates. The rates of H_2 production recorded for synthetic models of the hydrogenase enzyme reported to date are a lot lower than those of the enzyme. However, these systems offer the opportunity to explore and investigate the mechanisms of electrocatalysis, and by changing the coordinated ligands at the diiron centre and making substitutions to the dithiolate bridge the electrocatalytic properties can be tuned. With each novel synthetic analogue explored we are one step closer to a more efficient production of hydrogen and one step closer to a cleaner and more efficient energy source for tomorrow's world!

6.5 Bibliography

1 Shima, S., Pilak, O., Vogt, S., Schick, M., Stagni, M.S., Meyer-Klaucke, W., Warkentin, E., Thauer, R.K., Ermler, U., *Science*, **2008**, *321*, 572.

2 http://www.beyondfossilfuel.com/hydrogen/

3 *Platinum and Hydrogen for Fuel Cell Vehicles* (UK Department of Transport) available at http://www.dft.gov.uk/pgr/roads/environment/research/cqvcf/platinumandhydrogenforfuelce3838?page=3

4 Tard, C., Liu, X., Ibrahim, S.K., Bruschi, M., De Gioia, L., Davies, S.C., Yang, X., Wang, L., Sawers, G., Pickett, C.J., *Nature*, **2005**, *433*, 610.

5 Gloaguen, F., Rauchfuss, T.B., *Chem. Soc. Rev.*, **2009**, *38*, 100.

6 (a) Liu, T., Darensbourg, M.Y., *J. Am. Chem. Soc.*, **2007**, *129*, 7008, (b) Hu, X., Brunschwig, B.S., Peters, J.C., *J. Am. Chem. Soc.*, **2007**, *129*, 8988, (c) Gloaguen, F., Morvan, D., Capon, J.F., Schollhammer, P., Talarmin, J., *J. Electroanal. Chem.*, **2007**, *603*, 15, (d) Capon, J.F., Gloaguen, F., Schollhammer, P., Talarmin, J., *J. Electroanal. Chem.*, **2004**, *566*, 241, (e) Gloaguen, F., Lawrence, J.D., Rauchfuss, T.B., *J. Am. Chem. Soc.*, **2001**, *123*, 9476, (f) Borg, S.J., Behrsing, T., Best, S.P., Razavet, M., Liu, X., Pickett, C.J., *J. Am. Chem. Soc.*, **2004**, *126*, 16988, (g) Felton, G.A.N., Vannucci, A.K., Chen, J., Lockett, L.T., Okumura, N., Petro, B.J., Zakai, U.I., Evans, D.H., Glass, R.S., Lichtenberger, D.L., *J. Am. Chem. Soc.*, **2007**, *129*, 12521.

7 (a) Armstrong, F.A., *Curr. Opin. Chem. Biol.*, **2004**, *8*, 133, (b) Peters, J.W., Lanzilotta, W.N., Lemon, B.J., Seefeldt, L.C., *Science*, **1998**, *282*, 1853.

8 (a) Nicolet, Y., De Lacey, A.L., Vernede, X., Fernandez, V.M., Hatchikian, C.E., Fontecilla-Camps, J.C., *J. Am. Chem. Soc.*, **2001**, *123*, 1596, (b) Nicolet,

Y., Lemon, B.J., Fontecilla-Camps, J.C., Peters, J.W., *Trends Biochem. Sci.*, **2000**, *25*, 138.

9 Nicolet, Y., Piras, C., Legrand, P., Hatchikian, C.E., Fontecilla-Camps, J.C., *Structure*, **1999**, *7*, 13.

10 Pandey, A.S., Harris, T.V., Giles, L.J., Peters, J.W., Szilagyi, R.K., *J. Am. Chem. Soc.*, **2008**, *130*, 4533.

11 (a) Capon, J.F., Gloaguen, F., Pétillon, F.Y., Schollhammer, P., Talarmin, J., *Coord. Chem. Rev.*, **2009**, *253*, 1476, (b) Bruschi, M., Greco, C., Fantucci, P., De Gioia, L., *Inorg. Chem.*, **2008**, *47*, 6056.

12 Pierik, A.J., Hulstein, M., Hagen, W.R., Albracht, S.P.J., *Eur. J. Biochem.*, **1998**, *258*, 572.

13 Marken, F., Bond, A.M., Colton, R., *Inorg. Chem.*, **1995**, *34*, 1705.

14 (a) Justice, A.K., Linck, R.C., Rauchfuss, T.B., Wilson, S.R., *J. Am. Chem. Soc.*, **2004**, *126*, 13214, (b) Van der Vlugt, J.I., Rauchfuss, T.B., Whaley, C.M., Wilson, S.R., *J. Am. Chem. Soc.*, **2005**, *127*, 16012.

15 Barton, B.E., Rauchfuss, T.B., *Inorg. Chem.*, **2008**, *47*, 2261.

16 Ezzaher, S., Capon, J.F., Gloaguen, F., Pétillon, F.Y., Schollhammer, P., Talarmin, J., *Inorg. Chem.*, **2007**, *46*, 3426.

17 (a) Chong, D., Georgakaki, I.P., Mejia-Rodriguez, R., Sanabria-Chinchilla, J., Soriaga, M.P., Darensbourg, M.Y., *Dalton Trans.*, **2003**, 4158, (b) Liu, T., Wang, M., Shi, Z., Cui, H., Dong, W., Chen, J., Akermark, B., Sun, L., *Chem. Eur. J.*, **2004**, *10*, 4474, (c) Capon, J.F., Gloaguen, F., Schollhammer, P., Talarmin, J, *J. Electroanal. Chem.*, **2006**, *595*, 47, (d) Hon Cheah, M., Tard,

C., Borg, S.J., Liu, X., Ibrahim, S.K., Pickett, C.J., Best, S.P., *J. Am. Chem. Soc.*, **2007**, *129*, 11085.

18 Razavet, M., Davies, S.C., Hughes, D.L., Barclay, J.E., Evans, D.J., Fairhurst, S.A., Liu, X., Pickett, C.J., *Dalton Trans.*, **2003**, 586.

19 Darchen, A., Mousser, H., Patin, H., *J. Chem. Soc. Chem. Commun.*, **1988**, 968.

20 Gloaguen, F., Lawrence, J.D., Rauchfuss, T.B., Bénard, M., Rohmer, M.M., *Inorg. Chem.*, **2002**, *41*, 6573.

21 Morvan, D., Capon, J.F., Gloaguen, F., Le Goff, A., Marchivie, M., Michaud, F., Schollhammer, P., Talarmin, J., Yaouanc, J.J., *Organometallics*, **2007**, *26*, 2042.

22 Schmidt, M, Contakes, S.M., Rauchfuss, T.B., *J. Am. Chem. Soc.*, **1999**, *121*, 9736.

23 (a) Lyon, E.J., Georgakaki, I.P., Reibenspies, J.H., Darensbourg, M.Y., *Angew. Chem. Int. Ed.*, **1999**, *38*, 3178, (b) Windhager, J., Görls, H., Petzold, H., Mloston, G., Linti, G., Weigand, W., *Eur. J. Inorg. Chem.*, **2007**, 4462, (c) Windhager, J., Rudolph, M., Bräutigam, S., Görls, H., Weigand, W., *Eur. J. Inorg. Chem.*, **2007**, 2748, (d) Song, L.C., Yang, Z.Y., Bian, H.Z., Hu, Q.M., *Organometallics*, **2004**, *23*, 3082, (e) Song, L.C., Yang, Z.Y., Hua, Y.J., Wang, H.T., Liu, Y., Hu, Q.M., *Organometallics*, **2007**, *26*, 2106.

24 Apfel, U.P., Halpin, Y., Gottschaldt, M., Görls, H., Vos, J.G., Weigand, W., *Eur. J. Inorg. Chem.*, **2008**, *33*, 5112.

25 Apfel, U.P., Halpin, Y., Görls, H., Vos, J.G., Schweizer, B., Linti, G., Weigand, W., *Chemistry and Biodiversity*, **2007**, 2138.

26 Apfel, U.P., Kowol, C.R., Halpin, Y., Kloss, F., Kübel, J., Görls, H., Vos, J.G., Keppler, B.K., Morera, E., Lucente, G., Weigand, W., *J. Bioinorg. Chem.*, **2009**, *103*, 1236.

27 Teo, B.K., Hall, M.B., Fenske, R.F., Dahl, L.F., *Inorg. Chem.*, **1975**, *14*, 3103.

28 Tard, C., Liu, X., Hughes, D.L., Pickett, C.J., *Chem. Comm.*, **2005**, 133.

29 Bhugun, I., Lexa, D., Savéant, J.M., *J. Am. Chem. Soc.*, **1996**, *118*, 3982.

30 Best, S.P., Borg, S.J., White, J.M., Razavet, M., Pickett, C.J., *Chem. Comm.*, **2007**, 4348.

31 Ward, M.D., *Chem. Soc. Rev.*, **1995**, 121.

32 (a) Yu, Z., Wang, M., Li, P., Dong, W., Wang, F., Sun, L., *Dalton Trans*., **2008**, 2400, (b) Ezzaher, S., Orain, P.Y., Capon, J.F., Gloaguen, F., Pétillon, F.Y., Roisnel, T., Schollhammer, P., Talarmin, J., *Chem. Comm.*, **2008**, 2547.

33 (a) Gao, W., Ekström, J., Liu, J., Chen, C., Eriksson, L., Weng, L., Åkermark, B., Sun, L., *Inorg. Chem.*, **2007**, *46*, 1981, (b) Greco, C., Zampella, G., Bertini, L., Bruschi, M., Fantucci, P., De Gioia, L., *Inorg. Chem.*, **2007**, *46*, 108, (c) Liu, Z.P., Hu, P., *J. Chem. Phys.*, **2002**, *117*, 8177, (d) Song, L.C., Gao, J., Wang, H.T., Hua, Y.J., Fan, H.T., Zhang, X.G., Hu, Q.M., *Organometallics*, **2006**, *25*, 5724.

34 Glass, R.S., Gruhn, N.E., Lorance, E., Singh, M.S., Stessman, N.Y.T., Zakai, U.I., *Inorg. Chem.*, **2005**, *44*, 5728.